Neurobiology of Disease

Reduced Efficacy of the KCC2 Cotransporter Promotes Epileptic Oscillations in a Subiculum Network Model

Anatoly Buchin,[1,2,3] Anton Chizhov,[4,5] Gilles Huberfeld,[6,7] Richard Miles,[8] and Boris S. Gutkin[1,3]

[1]École normale supérieure, Paris Sciences et Lettres University, Laboratoire de Neurosciences Cognitives, Institute national de la santé et de la recherche médicale U960, Group for Neural Theory, 75005 Paris, France, [2]Peter the Great St. Petersburg Polytechnic University, St. Petersburg 195251, Russia, [3]National Research University Higher School of Economics, Center for Cognition and Decision Making, Moscow 109316, Russia, [4]Ioffe Institute, Computational Physics Laboratory, St. Petersburg 194021, Russia, [5]Sechenov Institute of Evolutionary Physiology and Biochemistry of the Russian Academy of Sciences, St. Petersburg 194223, Russia, [6]Université Pierre et Marie Curie, Pitié-Salpêtrière Hôpital, Assistance Publique–Hôpitaux de Paris, Neurophysiology Department, 75013 Paris, France, [7]Institute national de la santé et de la recherche médicale U1129 "Infantile Epilepsies and Brain Plasticity," Paris Descartes University, Pôle de recherche et d'enseignement supérieur Sorbonne Paris Cité, 75015 Paris, France, and [8]Institut du Cerveau et de la Moelle Epinière, Cortex et Epilepsie Group, 75013 Paris, France

Pharmacoresistant epilepsy is a chronic neurological condition in which a basal brain hyperexcitability results in paroxysmal hypersynchronous neuronal discharges. Human temporal lobe epilepsy has been associated with dysfunction or loss of the potassium-chloride cotransporter KCC2 in a subset of pyramidal cells in the subiculum, a key structure generating epileptic activities. KCC2 regulates intraneuronal chloride and extracellular potassium levels by extruding both ions. Absence of effective KCC2 may alter the dynamics of chloride and potassium levels during repeated activation of GABAergic synapses due to interneuron activity. In turn, such GABAergic stress may itself affect Cl^- regulation. Such changes in ionic homeostasis may switch GABAergic signaling from inhibitory to excitatory in affected pyramidal cells and also increase neuronal excitability. Possibly these changes contribute to periodic bursting in pyramidal cells, an essential component in the onset of ictal epileptic events. We tested this hypothesis with a computational model of a subicular network with realistic connectivity. The pyramidal cell model explicitly incorporated the cotransporter KCC2 and its effects on the internal/external chloride and potassium levels. Our network model suggested the loss of KCC2 in a critical number of pyramidal cells increased external potassium and intracellular chloride concentrations leading to seizure-like field potential oscillations. These oscillations included transient discharges leading to ictal-like field events with frequency spectra as *in vitro*. Restoration of KCC2 function suppressed seizure activity and thus may present a useful therapeutic option. These simulations therefore suggest that reduced KCC2 cotransporter activity alone may underlie the generation of ictal discharges.

Key words: **epilepsy; extracellular potassium; GABA; intracellular chloride; KCC2; subiculum**

Significance Statement

Ion regulation in the brain is a major determinant of neural excitability. Intracellular chloride in neurons, a partial determinant of the resting potential and the inhibitory reversal potentials, is regulated together with extracellular potassium via kation chloride cotransporters. During temporal lobe epilepsy, the homeostatic regulation of intracellular chloride is impaired in pyramidal cells, yet how this dysregulation may lead to seizures has not been explored. Using a realistic neural network model describing ion mechanisms, we show that chloride homeostasis pathology provokes seizure activity analogous to recordings from epileptogenic brain tissue. We show that there is a critical percentage of pathological cells required for seizure initiation. Our model predicts that restoration of the chloride homeostasis in pyramidal cells could be a viable antiepileptic strategy.

Introduction

Epilepsy is a chronic neurological disorder characterized by recurring seizures (Beghi et al., 2005; Fisher et al., 2005; Ullah and Schiff, 2009). GABAergic signaling is the main inhibitory system in the brain and its integrity is compromised in epilepsy. Intracellular chloride is maintained low so that when the $GABA_A$

Received Nov. 24, 2015; revised Aug. 4, 2016; accepted Aug. 7, 2016.

Author contributions: A.B., A.C., G.H., R.M., and B.S.G. designed research; A.B. and G.H. performed research; A.B., G.H., and R.M. contributed unpublished reagents/analytic tools; A.B., A.C., and G.H. analyzed data; A.B., A.C., G.H., R.M., and B.S.G. wrote the paper.

This work was supported by the following grants: ANR-10-LABX-0087 IEC, ANR-10-IDEX-0001-02 PSL, ERC-322721, FRM FDT20140930942. B.S.G. acknowledges partial support from Research Program 5-100 at the National Research University Higher School of Economics. The contribution of Anton Chizhov was supported by the Russian

receptor channel opens, chloride flows into neurons under the control of favorable concentration gradients despite unfavorable forces dictated by negative intracellular charges. Such accumulation results in an inhibitory hyperpolarization. Defects in chloride homeostasis may contribute to the epileptic activities generated in the tissue of patients with pharmacoresistant temporal lobe epilepsy associated with hippocampal sclerosis (Huberfeld et al., 2007) and in the cortical tissue surrounding tumors (Pallud et al., 2014). The expression or function of potassium-chloride transport proteins is altered in both these syndromes. The KCC2 cotransporter maintains basal chloride levels using ionic gradients created by the sodium-potassium pump to extrude intracellular chloride and potassium ions to the extracellular space (Payne et al., 2003). An absence of KCC2 has been correlated with a depolarizing shift in the resting reversal potential of GABAergic synaptic events in a minority of human subicular pyramidal cells (PYs Huberfeld et al., 2007). Experimental (Alger and Nicoll, 1982; Kaila and Voipio, 1987; Staley and Proctor, 1999) and theoretical studies (Doyon et al., 2011; Jedlicka et al., 2011) show that, in addition to basal effects, intense GABAergic stimulation leads to progressive chloride accumulation and therefore shifts the reversal potential to depolarized values. Thus, intensive activation of GABA synapses combined with impaired KCC2 cotransporter function may produce an aberrant proepileptic excitation.

In addition to chloride homeostasis, changes in extracellular potassium levels mediated via KCC2 may increase neuronal excitability and contribute to seizure generation (Fröhlich et al., 2008a). Potassium accumulation in the extracellular space is associated with seizures (Fertziger and Ranck, 1970) and spreading depression (Grafstein, 1956; Kraig and Nicholson, 1978). Intense neuronal firing should increase extracellular potassium further, increasing neuronal excitability in a positive feedback that promotes seizure generation. Recent computational models suggest that changes in extracellular potassium may suffice to induce seizure-like firing in single neurons (Hübel and Dahlem, 2014; Wei et al., 2014) or recurrent neural networks (Bazhenov et al., 2004; Ullah et al., 2009; Krishnan and Bazhenov, 2011).

However, relations between potassium-chloride transporters and dynamic changes in chloride and potassium levels during the transition to seizure are not completely understood. In this work, we therefore construct and validate a computational model incorporating realistic data on how KCC2 activity controls basal levels of chloride as a function of external potassium (Payne, 1997; Doyon et al., 2011). We use this model to explore how KCC2 controls dynamic changes in chloride levels due to GABAergic synaptic stimulation (Isomura et al., 2003; Fujiwara-Tsukamoto et al., 2007, 2010) and the effects of an absence of KCC2 actions. The model let us ask two questions: (1) Might normal KCC2 activity in some PYs have proepileptic actions mediated via an increase in extracellular potassium (Viitanen et al., 2010; Hamidi and Avoli, 2015)? and (2) Might an absence of KCC2 in other cells be proepileptic due to intracellular chloride accumulation with resulting depolarizing effects of GABA (Cohen et al., 2002; Huberfeld et al., 2007)?

We incorporated models of bursting PYs and interneurons (INs) of the subiculum into a neuronal network with realistic synaptic connectivity. Transport kinetics and exchange of both chloride and potassium between intraneuronal and extracellular space were explicitly modeled. Neuronal voltages were used to derive values for a local field potential (LFP) generated during normal and epileptic activity. Incorporating KCC2-deficient cells into this network reproduced ictal-like extracellular field potentials as in slices of human subiculum. Thus, our results support the hypothesis that a reduction in the effects of KCC2 in PYs may contribute to ictal activity and provide the basis for further experimental studies on the homeostasis of chloride in an epileptic context by PYs.

Materials and Methods

Epileptic tissue. Temporal lobe tissue blocks containing the hippocampus, subiculum, and part of the entorhinal cortex were obtained from 45 people of either sex with pharmacoresistant mesial temporal lobe epilepsies associated with hippocampal sclerosis (age, 18–52 years; seizures for 3–35 years) undergoing resection of the amygdala, the hippocampus, and the anterior parahippocampal gyrus. All of the individuals gave their written informed consent and the study was approved by the Comité Consultatif d'Ethique.

Tissue preparation. The postsurgical tissue was transported in a cold, oxygenated solution containing 248 mM D-sucrose, 26 mM $NaHCO_3$, 1 mM KCl, 1 mM $CaCl_2$, 10 mM $MgCl_2$ and 10 mM D-glucose, equilibrated with 5% CO_2 in 95% O_2. Hippocampal-subicular-entorhinal cortical slices or isolated subicular slices (400 μm thickness, 3 × 12 mm length and width) were cut with a vibratome (HM650 V, Microm). They were maintained at 37°C, and equilibrated with 5% CO_2 in 95% O_2 in an interface chamber perfused with a solution containing 124 mM NaCl, 26 mM $NaHCO_3$, 4 mM KCl, 2 mM $MgCl_2$, 2 mM $CaCl_2$, and 10 mM D-glucose. NBQX and D,L-AP5 were used to block glutamatergic signaling, and bicuculline or picrotoxin was used to block $GABA_A$ receptors. Ictal-like activity was induced by increasing the external K^+ concentration to 8 mM and reducing the Mg^{2+} concentration to 0.25 mM.

Recordings. Up to four tungsten electrodes etched to a tip diameter of ~5 μm were used for the extracellular recordings. The signals were amplified 1000-fold and filtered to pass frequencies of 0.1–10 kHz (AM Systems, 1700). The intracellular recordings were made with glass microelectrodes containing 2 M potassium acetate and beveled to a resistance of 50–100 MΩ. The signals were amplified with an Axoclamp 2B amplifier in current-clamp mode. The intracellular and extracellular signals were digitized at 10 kHz with a 12 bit, 16-channel analog-to-digital converter (Digidata 1200A, Molecular Devices), and monitored and saved to a PC with AxoScope (Molecular Devices).

Data analysis. Records were analyzed with Clampfit 10 software and scripts written in Matlab (2015a).

Simulations. Single-neuron and neural-network simulations were performed in Matlab (2015a) using the direct Euler method of integration, with a time step of 0.05 ms. We checked that smaller time steps provided substantially similar results. Bifurcation analysis was performed in XPPAUT 7.0 and the Auto package. In all simulations, initial conditions were systematically varied to check stability of numerical results. The model code is available on Model DB (https://senselab.med.yale.edu/modeldb/).

Neuron intrinsic properties. Single-neuron activity was modeled using the conductances derived from previous studies (Mainen and Sejnowski, 1996; Krishnan and Bazhenov, 2011). The intrinsic currents selected represent the major currents needed to reproduce the firing patterns of subicular PYs (Staff et al., 2000; Jung et al., 2001). We used a model of a regular-spiking neuron for the PYs and a fast-spiking neuron for the INs (Mainen and Sejnowski, 1996; Bazhenov et al., 2004). To take into account the activation of bursting properties of PYs due to increased extracellular potassium (Jensen et al., 1994), the intrinsic potassium currents were modulated by its concentration in a manner similar to that reported by Fröhlich et al. (2008b).

Foundation for Basic Research with the Research Projects 15-29-01344,15-04-06234, and 16-04-00998. We thank Maxim Bazhenov, Giri Krishnan, and Sergei Prokhorenko for fruitful discussions.

The authors declare no competing financial interests.

Correspondence should be addressed to Anatoly Buchin, 29, rue d'Ulm, 75005 Paris, France. E-mail: anat.buchin@gmail.com.

DOI:10.1523/JNEUROSCI.4228-15.2016

The following equations describe the evolution of voltage over time for somatic and dendritic compartments:

$$C_m dV_d/dt = -I_d^{Int} - g_c^d(V_d - V_s) - I_d^{leak} - I_d^{pump}$$

$$g_c^d(V_d - V_s) = -I_s^{Int} - I_s^{leak} - I_s^{pump}$$

V_d is the voltage of the dendritic compartment; $C_m = 0.75\ \mu F/cm^2$; I_d^{leak} includes sodium, potassium, and chloride leak currents (PYs: $g_k = 0.044$, $g_{Na} = 0.02$, $g_{Cl} = 0.01$ mS/cm^2; INs: $g_k = 0.035$, $g_{Na} = 0.02$, $g_{Cl} = 0.01$ mS/cm^2); and I_s^{leak} includes sodium and potassium leak currents (PYs: $g_{Na} = 0.019$, $g_k = 0.042$ mS/cm^2; INs: $g_{Na} = 0.019$, $g_k = 0.042$ mS/cm^2). I_d^{Int} and I_s^{Int} are the sums of intrinsic currents for axosomatic and dendritic compartments, respectively. I_d^{pump} and I_s^{pump} are the sums of the Na^+ and K^+ ion currents (I_{Na}^{pump}, I_K^{pump}) carried by the Na^+-K^+ pump for somatic and dendritic compartments. The compartments were coupled by an axial current (PYs: $g_c = 1.65\ \mu S$; INs: $g_c = 0.5\ \mu S$; $S_{soma} = 1 \times 10^{-6}$ cm^2, $S_{dend} = 165 \times 10^{-6}$ cm^{-2}). Axosomatic currents were assumed to be sufficiently strong to change the somatic membrane voltage instantaneously, so the axosomatic compartment has no capacitance current. Current carried by the sodium-potassium pump was dependent on intracellular sodium (Na_{IN}^+) as well as extracellular potassium (K_{OUT}^+) concentrations given by the following equations (Kager et al., 2000):

$$A = 1/(1 + K_{o\alpha}/K_{OUT}^+)^2/(1 + Na_{i\alpha}/Na_{IN}^+)^3$$

$$I_{Na-K}^{pump} = -2I_{Na-K}^{max}A + 3I_{Na-K}^{max}A$$

where $K_{oa} = 3.5$ mM, $Na_{i\alpha} = 20$ mM, $Na_{IN}^+ = 20$, and $I_{Na-K}^{max} = 25\ \mu A/cm^2$.

The sum of intrinsic currents for the dendritic compartment was given by $I_d^{Int} = I_{HVA} + I_{KCa} + I_{Km} + I_{Nap} + I_{Na}^d + I_{Ca} + I_d^{pump} + I_d^c + I_d^{leak}$ currents for the PYs and by $I_d^{Int} = I_d^{pump} + I_d^c + I_d^{leak}$ currents for INs. Intrinsic currents for the somatic compartment are described as $I_d^{Int} = I_d^{pump} + I_d^c + I_d^{leak}$ for both PYs and INs, where I_s^{Int} consists of the voltage-gated sodium (PYs and INs: $G_{Na} = 3450$ mS/cm^2) and delayed-rectifier potassium ($G_{K\nu} = 200$ mS/cm^2) currents. The dendritic compartment for PYs had a high-threshold calcium current (I_{HVA}), a calcium-activated potassium current (I_{KCa}), a calcium current (I_{Ca}), a slowly activating potassium current (I_{Km}), voltage-gated and persistent-sodium currents (I_{Na} and I_{Nap}, respectively; Jung et al., 2001), and leak conductances (PYs: $G_K = 0.044$, $g_{Na} = 0.02$, $g_{Cl} = 0.01$ mS/cm^2; INs: $G_K = 0.035$, $G_{Na} = 0.02$, $G_{Cl} = 0.035$ mS/cm^2). Full approximations of these currents have been described (Mainen and Sejnowski, 1996; Krishnan and Bazhenov, 2011).

Ion concentration dynamics. We modeled variations in Ca_{IN}^{2+}, K_{OUT}^+, and Cl_{IN}^- levels, leak currents, intrinsic currents, pump-mediated currents, extracellular diffusion, and glial activities, which affected ionic homeostasis. The Nernst equation was used to determine reversal potentials for potassium and chloride from internal and external concentrations for each ion. These ionic levels were calculated from active currents, activities of the sodium-potassium pump, and the KCC2 cotransporter (Doyon et al., 2011), as well as ion flow between PYs and through extracellular space (Wei et al., 2014). We followed the assumption that the activity of the Na-K pump is regulated by extracellular potassium in neurons (Kager et al., 2000) and glia (Grisar, 1984). External potassium, K_{OUT}^+, was modeled as reported by Krishnan and Bazhenov, (2011), and a two-dimensional network was used to model extracellular diffusion, taking into account the cortical structure of subiculum. The intracellular potassium was set at $K_{IN}^+ = 150$ mM. We applied the following equations:

$$dK_{OUT}^+/dt = (k_K/Fd)(\Sigma I_K^{int} + I_{Na-K}^{pump} - I_{KCC2}) + G$$

$$+ \sum_{i=1}^{4} D_{ij}/\Delta x^2(K_{OUT}^+ - K_{OUT}^{+(i)}) + d_{bath}/\Delta l^2(K_{OUT}^+ - K_{bath})$$

where the glial uptake G was modeled the same way as that described by Kager et al. (2007) according to the following equations:

$$G = k_{ON}/k_{1N}(B_{max} - B) - k_{OFF}K_{OUT}^+B$$

$$dB/dt = k_{OFF}(B_{max} - B) - k_{ON}K_{OUT}^+B$$

where the conversion factor $k = 10 \times 10^3$ cm^3, $F = 96{,}489$ C/mol, and the ratio between the cell volume and extracellular volume $d = 0.15$. D_{ij} is an element of diffusion matrix D, and $D_{ij} = 4 \times 10^{-6}$ cm^2/s for neighboring neurons (cat neocortex data; Fisher et al., 1976) and $D_{ij} = 0$ otherwise. Since subiculum PYs are organized in layers of a few millimeters depth, we have chosen a two-dimensional diffusion model, which made it possible to save significantly on computational requirements without jeopardizing the main results of the paper. The first-order diffusion approximation efficiently takes into account the spread of potassium in the cortical layer from 0.8 mm up to 3 mm depth (Fisher et al., 1976). Each subicular PY has four neighboring cells with a mean distance of $\Delta x = 50\ \mu m$ between their somata (Huberfeld et al., 2007); $d_{bath} = 4 \times 10^{-7}$ Hz is the coefficient for diffusion from the bath (Cressman et al., 2009; Florence et al., 2009; Barreto and Cressman, 2011) and $\Delta l = 200\ \mu m$ is the depth of the neurons in the slice. The bath K_{OUT}^+ concentration was assumed to be uniform in the network and to equilibrate very rapidly (Bazhenov et al., 2004). Glial K_{OUT}^+ uptake was modeled by free buffer (with total capacity $B_{max} = 500$ mM) with a concentration B, which bound and unbound from K_{OUT}^+ with first-order kinetics, and the rates k_{ON} and k_{OFF} were given by $k_{ON} = 0.008$ and $k_{OFF} = k_{ON}/(1 + \exp(-(K_{OUT}^+ - K_{oth}^+)/1.15))$ (Kager et al., 2007; Volman et al., 2007). The spatial buffering via gap junctions was not modeled since it has been found that K_{OUT}^+ clearance does not strongly depend on connections between the astrocytes (Wallraff et al., 2006). Changes in K_{OUT}^+ due to the INs were assumed to be negligible compared with the K_{OUT}^+ produced by the PYs. Changes in K_{OUT}^+ due to extrusion from PYs were assumed to affect both PYs and INs. In some simulations, extracellular diffusion from the bath to neurons was set to zero to mimic *in vivo* conditions. In simulations without KCC2 contribution to K_{OUT}^+ [$I_{KCC2}(-)$ cells] parameter I_{KCC2}^{max} was set to zero in K_{OUT}^+ equation but was still present for Cl_{IN}^-.

Extracellular chloride concentration is assumed to be constant: $Cl_{OUT}^- = 130$ mM. Intracellular chloride Cl_{IN}^- concentration was calculated from the following equations:

$$dCl_{IN}/dt = (k_{Cl}/F)(I_D^{Cl} + I_{GABA} + I_{KCC2})$$

$$I_{KCC2} = I_{KCC2}^{max}(V_K - V_{Cl})/((V_K - V_{Cl}) + V_{1/2})$$

where I_D^{Cl} is the chloride leak current on the dendrite, $I_{KCC2}^{max} = 2\ \mu A/cm^2$ is the maximal current through the KCC2 cotransporter, V_K and V_{Cl} are the reversal potentials of potassium and chloride, $V_{1/2} = 40$ mV is the voltage difference when the chloride-potassium current reaches half-maximum velocity, and $I_{GABA} = \sum_i g_{GABA}^i s_{GABA}^i(V - V_{GABA})$ is the sum of GABAergic currents received by a neuron. Using the conductance-based GABA synapse model and chloride leak current allows us to take into account the depolarization-driven uptake of intracellular chloride.

The outgoing flux via KCC2 was modeled according to the examples of Doyon et al., (2011, 2016), Staley et al. (1995), and Staley and Proctor (1999). The current via KCC2 describes the flow of potassium and chloride ions from the intracellular to the extracellular space. Both these currents are assumed to be equal in the absolute value, but opposite in polarity so that the net current is zero. I_{KCC2} describes the currents of potassium and chloride ions via the KCC2 cotransporter, which could flow in either direction, depending on the sign of free energy proportional the voltage difference $V_K - V_{Cl}$ (Staley and Proctor, 1999). The value of half-maximum velocity $V_{1/2}$ of the KCC2 pump corresponds to the assumption that Cl_{IN}^- increased ≤15 mM and Cl_{OUT}^- decreased ≤120 mM, while $V_K = -95$ mV (Doyon et al., 2011).

Intracellular calcium dynamics was modeled with the following equation:

$$dCa_{IN}^{2+}/dt = -(5.18 \times 10^{-5})/D_{ca}I_{HVA} + (2.4 \times 10^{-4} - Ca_{IN}^{2+})/\tau_{Ca}$$

where $\tau_{Ca} = 800$ ms and $D_{Ca} = 0.85$ cm$^2 \times$ mM/μA.

Reversal potentials for each current were calculated from the Nernst equation and continuously updated with internal and external ion concentrations on every time step:

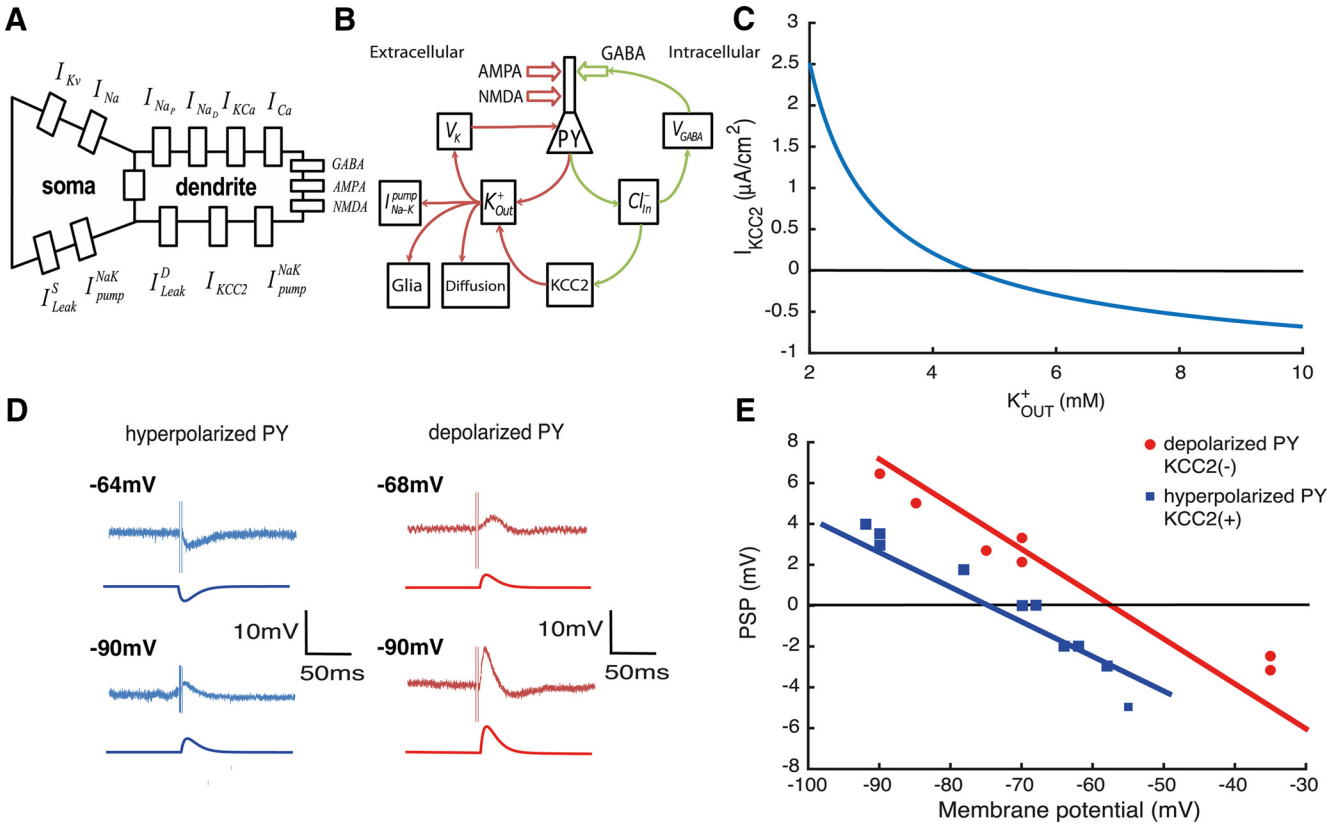

Figure 1. Absence of KCC2 leads to a depolarizing GABA reversal potential. ***A***, Scheme of the PY model with intrinsic currents. ***B***, Ionic pathways in the single-cell model. ***C***, Current via KCC2 cotransporter I_{KCC2} as function of extracellular potassium K^+_{OUT} when $Cl^-_{IN} = 4$ mM and $I^{max}_{KCC2} = 2\ \mu A/cm^2$. ***D***, Experimental and model voltage traces during GABAergic stimulation. ***E***, Amplitude of the PSP during experimental stimulation (red and blue dots) and in the model (red and blue lines). Experimental traces of ***D*** and ***E*** are taken from Cohen et al. (2002).

$$V_K = \frac{RT}{F}\ln\left(\frac{K^+_{OUT}}{K^+_{IN}}\right),\ V_{Cl} = \frac{RT}{F}\ln\left(\frac{Cl^-_{IN}}{Cl^-_{OUT}}\right) \text{ and}$$

$$V_{GABA} = \frac{RT}{F}\ln\left(\frac{4Cl^-_{IN} + HCO^-_{3IN}}{4Cl^-_{OUT} + HCO^-_{3OUT}}\right),$$

where $HCO^-_{3IN} = 16$ mM and $HCO^-_{3OUT} = 26$ mM (Doyon et al., 2011).

Network and synaptic model. The subiculum network was modeled with 841 PYs and 225 INs, to give a ratio close to 80% excitatory and 20% inhibitory cells. Increasing the size of the network had a minimal effect on the network dynamics. Synaptic connectivity between cells was made at random at levels based on estimates from the mouse subiculum measured at standard potassium concentrations (Böhm et al., 2015) as follows: $P_{PY-PY} = 0.05$, $P_{IN-PY} = 0.65$, $P_{PY-IN} = 0.3$, $P_{IN-IN} = 0.4$. Peak conductances at simulated synapses varied according to the normal distribution with the following means: PY–PY: 1.5 nS/cm^2 for AMPA and 0.02 nS/cm^2 for NMDA; PY–IN: 1 nS/cm^2 for AMPA; IN–PY: 0.7 nS/cm^2 for GABA; and IN–IN: 0.5 nS/cm^2 for GABA and a variance at 10% of the corresponding mean. Synaptic parameters were systematically varied to ensure stability of network activity. Both PYs and INs also received a noisy excitatory synaptic input (AMPA) to induce spontaneous firing. Additional AMPA synaptic currents were modeled by an Ornstein–Uhlenbeck process (Renart et al., 2007) expressed as follows: $\tau_{AMPA}\frac{dI_{AMPA}}{dt} = -I_{AMPA} + \sigma_{E/I}\eta(t)$, where $\tau_{AMPA} = 5.4$ ms, $\sigma_E = 0.50$ μA/cm^2 and $\sigma_I = 0.60$ μA/cm^2. The time course of currents at simulated AMPA, NMDA, and GABA synapses followed first-order kinetics, similar to those used by Brunel and Wang (2001).

LFP model. We computed an LFP from the summed activity of neurons of the simulated network. PYs were assumed to provide the largest component of the LFP signal (Buzsáki et al., 2012). Each PY i generated a dipole $\varphi_i = -k(V^i_d - V^i_s)$ (Chizhov et al., 2015) as reported by Demontis-Guignard et al. (2012) and Wendling et al. (2012), where $k = 0.02$ is the proportionality coefficient for the PY layer. A global LFP signal was computed as a superposition assuming all PYs contribute equally, expressed as follows: $LEP = 1/N\sum_i \varphi_i$.

Seizure detection algorithm. Seizure-like events in the simulated field activity were detected with an algorithm that estimated the total power spectrum over a time window of 5 s. Events exceeding an amplitude threshold were classified as seizures.

Results

Absence of KCC2 leads to a depolarizing GABA reversal potential

PYs with associated intrinsic and synaptic conductances of somatic and dendritic compartments were modeled (Fig. 1*A*). Active currents include the calcium-dependent potassium conductances that contribute to burst firing in subicular PYs (Stanford et al., 1998; Jung et al., 2001). Random synaptic currents mediated by AMPA and NMDA receptors initiate firing in the model cell and each action potential induces an increase in extracellular potassium. Major ion pathways associated with potassium and chloride homeostasis are shown in Figure 1*B*. K^+_{OUT} affects the reversal potential of all potassium currents and so modulates the excitability of the neuron model. The sodium-potassium pump, glial buffering, and extracellular diffusion to the neighboring cells restore potassium levels toward the original value of ~3.35 mM. With these homeostatic mechanisms, we found ion concentrations in the model reached a stable equilibrium at physiological levels.

Activation of GABAergic synapses increases intracellular chloride concentrations Cl^-_{IN} in the model (Fig. 1*B*). Intracellular

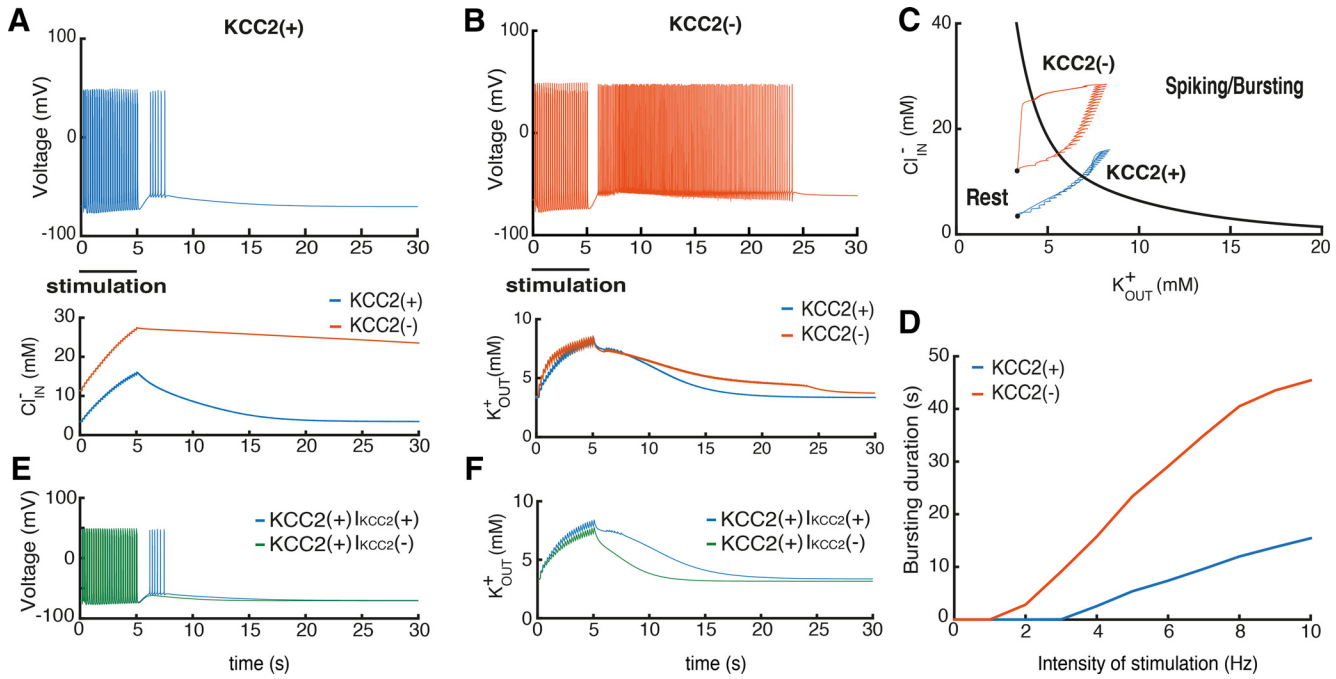

Figure 2. Consequences of the KCC2(−) pathology in single PYs. ***A***, ***B***, voltage trajectories of the KCC2(−) and KCC2(+) PY neurons after stimulation with periodic AMPA, GABA, and NMDA synaptic input for 5 s. Bottom, Changes in K^+ and Cl^- levels. ***C***, State diagram of the model and changes in ionic concentrations. Red and blue trajectories correspond to the KCC2(−) and KCC2(+) cells, respectively. ***D***, Relations between stimulus intensity and firing after stimulation for KCC2(−) (red) and KCC2(+) (blue) cells. ***E***, Voltage trajectories of the KCC2(+) with and without KCC2 contribution to the extracellular potassium after the same synaptic stimulation as in ***A*** [KCC2(+) $I_{KCC2}(+)$ and KCC2(+) $I_{KCC2}(-)$]. ***F***, The corresponding extracellular potassium concentration changes.

chloride levels are then restored by activity of the KCC2 cotransporter, which extrudes chloride and potassium ions into extracellular space. The KCC2 cotransporter current depends on K^+_{OUT} (Fig. 1*C*). At large values of K^+_{OUT}, the KCC2 cotransporter current could reverse the direction and load neurons with chloride (Payne, 1997). The increase in internal chloride levels leads to higher V_{GABA} values and so decreases the efficacy of inhibition.

Baseline intracellular chloride levels in the model cell depend on KCC2 activity. In KCC2(+) cells, they tend to return to ~3.5 mM, corresponding to a GABA reversal potential of $V_{GABA} = -78$ mV, with an associated neuronal resting potential of −70 mV. In model cells with no KCC2 actions [KCC2(−)] internal chloride stabilizes at 11.3 mM, corresponding to $V_{GABA} = -56$ mV, with an associated resting potential of −65 mV. The absence of KCC2 thus results in a depolarizing GABA reversal potential and an depolarized resting membrane potential due to the chloride leak currents (Jedlicka et al., 2011; Krishnan and Bazhenov, 2011).

According to our model, the value of V_{GABA} in KCC2(−) and KCC2(+) cells is the result of intracellular chloride concentration levels CL^-_{IN}. V_{GABA} is determined by joint concentration of chloride Cl^- and bicarbonate HCO_3^- ions inside and outside of the cell (see Materials and Methods). Thus the presence of the HCO_3^- component makes V_{GABA} significantly higher than V_{Cl} (Payne et al., 2003), while the value of V_{Cl} is equal to the membrane potential.

The PY model was stimulated with a GABA conductance to ask how internal chloride levels affect GABAergic signaling (Fig. 1*D*). The GABAergic synaptic current was modeled with second-order synaptic kinetics (Chizhov, 2002) and no excitatory input was modeled (Cohen et al., 2002). The dependence of GABA currents on KCC2 actions is shown by plotting the amplitude of the postsynaptic potential (PSP) as a function of membrane potential (Fig. 1*E*, experimental and model traces). The same GABAergic stimulus induces a hyperpolarization in the KCC2(+) PY, but depolarizes the KCC2(−) cell. The blue and red lines are predictions of PSP amplitude from the model. The absence of the KCC2 cotransporter results in a difference of ~20 mV in the reversal potential of the response to GABA.

Single-cell consequences of KCC2(−) pathology

We next asked how KCC2 influences excitability by exploring responses of the model cell to synaptic stimuli in the absence of extracellular diffusion. The stimulation protocol was developed to reproduce seizure-like events in rat hippocampal slices (Fujiwara-Tsukamoto et al., 2007, 2010) and in epileptic human hippocampal slices (Huberfeld et al., 2011). AMPA, GABA, and NMDA conductances in KCC2(+) or KCC2(−) neurons were activated for 5 s at 5 Hz (Fig. 2*A*,*B*). This simulated synaptic stimulation provoked a sustained bursting afterdischarge activity, which was prolonged after the stimulus stopped. Bursting activity in the KCC2(+) cell took less time (Fig. 2*A*) than bursting activity in the KCC2(−) cell, which lasted for several hundred milliseconds (Fig. 2*B*). A slow depolarization after stimulation in both cells resulted from the excitatory effect of extracellular potassium accumulation.

We explored how changes in potassium and chloride levels contribute to sustained after-discharges in model neurons in a bifurcation analysis using levels of these ions as control parameters. The resulting state diagram (Fig. 2*C*) shows how the intracellular chloride Cl^-_{IN} and extracellular potassium K^+_{OUT} concentrations affect neuron behavior. The black line figures the border between regions of firing or silence in the model neuron. It corresponds to a line of saddle-node bifurcations in the two-parameter diagram. Thus, high levels of K^+_{OUT} and Cl^-_{IN} move the neuron into the burst firing regime. In KCC2(−) cells, elevated internal chloride Cl^-_{IN} provides an additional depolarization via

effects on chloride leak current reversal potential (Krishnan and Bazhenov, 2011). Thus an absence of KCC2 increases excitability by moving neuronal potential toward the firing region of the state diagram (Fig. 2*C*).

The enhanced excitability of the KCC2(−) neuron affects how it respond to synaptic stimulation. K^+_{OUT} and Cl^-_{IN} increase due to spiking and GABAergic stimulation and, when ionic concentrations increase sufficiently, the cell moves into the region of spiking/bursting (Fig. 2*C*). When KCC2 is active, however, the accumulation of intracellular chloride was much reduced. The same synaptic stimulation moved the cell KCC2(+) less far into the spiking/bursting region of the state plot. The time to restore baseline ionic homeostasis in the KCC2(−) cell was longer than in the control neuron, resulting in a long after-discharge before the membrane potential returned to baseline (Fig. 2*C*, black dots).

We then explored how the absence of KCC2 affects responses to different intensities of synaptic stimulation. In KCC2(−) cells, compared to KCC2(+) cells, the minimal stimulation intensity needed to evoke spiking during slow depolarization was less and the duration of the afterdischarge was longer for all frequencies. In summary, when KCC2 actions are suppressed, PYs generate bursting activity more easily due to larger amount of depolarization provided by chloride leak current because of increased Cl^-_{IN} concentration.

Since KCC2 affects both K^+_{OUT} and Cl^-_{IN}, it is important to separate these two contributions for single-neuron excitability. For this purpose, we performed simulations with KCC2(+) cell when the K^+_{OUT} level depends on KCC2 activity, $I_{KCC2}(+)$, and does not depend on $I_{KCC2}(-)$ (see Materials and Methods). We found that in the $I_{KCC2}(+)$ case, the synaptic stimulation similar to Figure 2*A* leads to the substantial depolarization triggering the spiking activity (Fig. 2*E*), while in the $I_{KCC2}(-)$ case the depolarization is smaller. Analysis of ion concentration changes after the stimulation showed that $I_{KCC2}(+)$ cells provide a substantially higher amount of K^+_{OUT} compared with $I_{KCC2}(-)$ (Fig. 2*F*). The difference between these curves corresponds to the amount of K^+_{OUT} released uniquely by the KCC2 cotransporter after synaptic stimulation. This additional K^+_{OUT} increase caused larger depolarization leading to the spiking activity in the $I_{KCC2}(+)$ cell (Fig. 2*E*).

We found that the amount of excessive K^+_{OUT} released by KCC2 could trigger spiking activity in the KCC2(+) case after application of the synaptic stimulation, while in the stationary case the presence of the cotransporter in KCC2(+) cells does not provide the substantial increase of K^+_{OUT} concentration (Fig. 2*C*). The paradoxical effect of KCC2 is observed because the cotransporter operates close to the thermodynamic equilibrium where V_K is close to V_{Cl} (Payne et al., 2003), thus making the current passing via KCC2 very small. Therefore, there is no substantial difference between KCC2(−) and KCC2(+) cells in terms of K^+_{OUT} concentration. Yet the situation changes dramatically once the ion concentrations of K^+_{OUT} and Cl^-_{IN} and the corresponding reversal potentials are increased (Fig. 2*F*). In this case, the additional amount of K^+_{OUT} passing through KCC2 provides substantial depolarization leading to spiking (Fig. 2*E*), similar to the experiments by Viitanen et al. (2010).

Since the interaction between K^+_{OUT} and neural excitability depends on multiple mechanisms, we performed simulations to clarify each specific contribution. Glial buffer and I^{pump}_{Na-K} have different dependence on K^+_{OUT} (Fig. 3*A*,*B*) and therefore should have a different effect on ion regulation. To clarify their contribution, we stimulated the KCC2(+) cell with a burst induction stimulus (same stimuli as in Fig. 2*A*). Blocking the various K^+_{OUT} mechanisms led to changes in the I_{KCC2} current, during the K^+_{OUT} increase induced by stimulation (Figs. 2*B*, 3*C*). We found that removal of the glial buffer substantially increases neural excitability leading to longer after-depolarization and more afterdischarges (Fig. 3*D*). Removing the sodium-potassium pump contribution, at constant sodium concentration, has even more dramatic effects on single-neuron dynamics. At the end of the stimulation, the KCC2(+) neuron fires continuously due to extracellular potassium accumulation (Figs. 2*B*, 3*D*), while the glial buffer is not fast enough to compensate. Based on these simulations we conclude that both I^{pump}_{Na-K} and glial buffer have a large effect on K^+_{OUT} regulation and corresponding excitability changes, yet I^{pump}_{Na-K} provides the major contribution.

Gamma oscillations in KCC2(+) subiculum network model

We next asked how these KCC2-dependent changes in potassium and chloride homeostasis and the resulting alterations in neuronal excitability affect network behavior. Network oscillations were examined in a subiculum network consisting of GABAergic two-compartment INs and PYs as described in Materials and Methods. PY and IN neurons were sparsely connected by conductance-based synapses with realistic subiculum connectivity (Böhm et al., 2015). Parameters used at these synapses were adjusted to physiologically realistic values. All neurons in the network were exposed to the same K^+_{OUT} ion concentration, which affected both the PYs and the INs, and the dynamics of chloride concentrations Cl^-_{IN} in PYs were identical.

We examined responses of the network to protocols similar to those used experimentally to evoke pathological bursting discharges (cf. Huberfeld et al., 2011). With an excitation equivalent to that provided by 8 mM potassium and 0.5 mM magnesium in the external solution (Huberfeld et al., 2011), activity of the network model became organized into stable oscillations (Fig. 4*A*) at a peak frequency of ~36 Hz. This gamma frequency oscillation is similar to that recorded from the subiculum *in vitro* (Colling et al., 1998; Stanford et al., 1998; LeBeau et al., 2002; Huchzermeyer et al., 2008; Jackson et al., 2011). The increased potassium concentrations provide significant excitation to both PYs and INs, thus contributing to the population oscillations. At levels equivalent to 4 mM potassium, the network activity organizes into sparse random firing. We ensured that stable gamma oscillations exist in the network in the absence of the additional extracellular potassium from the bath, when PY and IN populations receive sufficient external excitation (simulations not shown).

Both extracellular potassium and intracellular chloride levels increase during simulated gamma oscillations. At a steady state after 1–2 min of simulated oscillations, K^+_{OUT} reached an equilibrium at 7.9 mM and Cl^-_{IN} was 8.6 mM (Fig. 4*C*). We note local increases in K^+_{OUT} during spiking, which tend to equilibrate quickly after each spike, and also small oscillations during each cycle of network activity. Thus, the oscillations generated by the PY–IN network led to quasistationary ion levels and a physiological type of population activity.

Synchronous PY firing during the gamma oscillations led to oscillations of our computed LFP (Fig. 4*D*). While single PYs did not fire on each cycle of the oscillation, the overall PY population activity fluctuated with the LFP oscillations (Fig. 4*B*). In contrast, inhibitory cells tended to fire a spike on every oscillation cycle with a strong peak at ~36 Hz (Fig. 4*D*). Such firing interplay has been described as a PY–IN network gamma mechanism (Whittington et al., 2000).

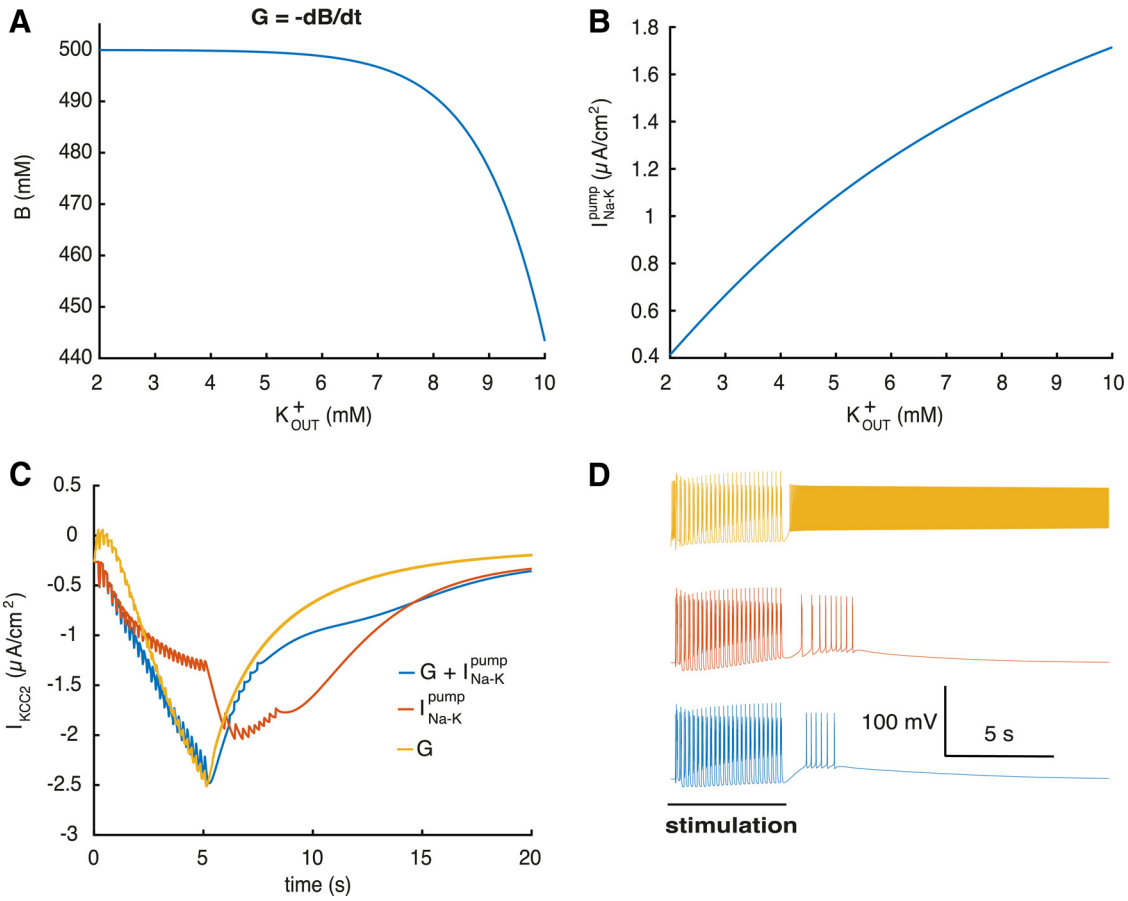

Figure 3. Mechanisms of extracellular potassium regulation. ***A***, Capacity of the glial buffer depending on K^+_{OUT}. ***B***, Current via I^{pump}_{Na-K} depending on K^+_{OUT}. ***C***, Current via KCC2 when different K^+_{OUT} regulation mechanisms are present in the KCC2(+) cell. ***D***, Corresponding voltage traces (same stimulus as in Fig. 2 *A*, *B*).

KCC2(−) pathology in the subiculum circuit

By constructing networks with a varying proportion of KCC2-deficient PYs, we studied how KCC2(−) cells might contribute to seizure initiation. All neurons in simulated networks were excited by an equivalent external potassium level of 8 mM to reflect previous work (Huberfeld et al., 2011). Effective extracellular potassium levels were dependent on this excitation and also on the potassium extruded by neuronal firing. We assumed KCC2(−) PYs were not clustered in simulated network space and performed additional simulations to check that such clusters did not affect results (simulations not shown). The initial conditions were set at baseline ionic levels for KCC2(−) and KCC2(+) cells, calculated from the single-neuron model (Fig. 2*C*).

The addition of 30% of KCC2(−) PYs to the simulated network provoked synchronous population bursting similar to ictal discharges (Fig. 5*A*). PY firing due to elevated chloride levels in these KCC2(−) cells led to a substantial activation of IN cells and a strong recurrent GABAergic input to PYs. With a depolarized GABAergic reversal potential, KCC2(−) cells did not receive an effective inhibition, and tended to discharge more strongly than KCC2(+) cells.

We next compared LFPs generated by the simulated network with those recorded from human subicular tissue during the transition to ictal activity (Fig. 5*B*). As in experimental records, the model initially generated a weakly synchronous activity that gradually shifted into more synchronous periodic population bursting (Fig. 5*A*). Initial fast oscillations in the simulated LFP result from strong PY firing and are then transformed into population burst firing at 4 Hz (Fig. 5A), as demonstrated experimentally (Fig. 5B, insets). We noted a number of nonperiodic synchronous population bursts being generated by the model before the onset of the seizure (Fig. 5*B*, asterisk). These irregular discharges occurred as the network approached an ictal state characterized by periodic bursting.

In the network, these discharges were initiated by recurrent AMPA-mediated synaptic events and terminated by cellular Ca^{2+}-dependent potassium currents. A close analysis of simulated activity revealed the following sequence of events. Random excitatory inputs in the KCC2(−) group of PYs initiate firing in other neurons via recurrent excitatory synapses, which tends to trigger Ca^{2+}-dependent potassium currents and so stops firing in PYs that participate in the initial aperiodic population bursts (Fig. 5*B*, asterisk). With a random initiation, the irregular character of these discharges (Jirsa et al., 2014) gradually transforms into the periodic bursting activity specific for ictal discharges.

During transition to the ictal state, an enhanced excitation from KCC2(−) PYs activated IN cells, leading to a strong repetitive activation of GABAergic synapses. Consequences include an increase of intracellular chloride levels Cl^-_{IN} in PYs and of K^+_{OUT} levels in the extracellular space due to the increased firing (Fig. 5*C*). While the increase in extracellular potassium during the transition was buffered by rapid diffusion, the intracellular chloride in both KCC2(−) and KCC2(+) cells increased significantly. The GABAergic reversal potential was considerably depolarized and an effective positive feedback loop between

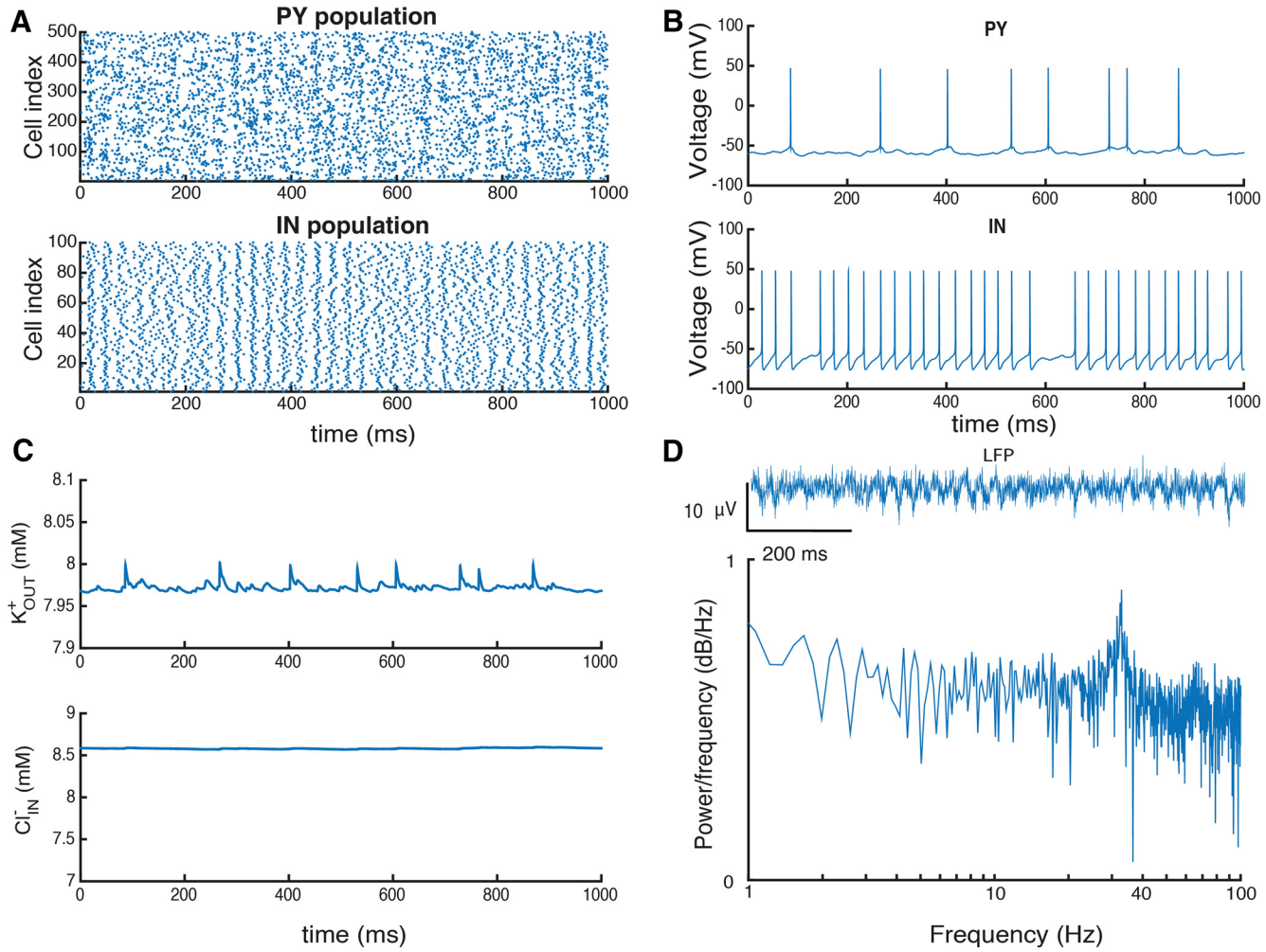

Figure 4. Ion concentrations during gamma oscillations in the PY–IN network in the presence of 8 mM potassium in the bath solution. ***A***, Raster plot showing activity for a representative part of the PY and IN populations. ***B***, Voltage traces from representative PYs and IN cells. ***C***, K^+_{OUT} and Cl^-_{IN} concentrations during network activity. ***D***, LFP computed from PY activity and, below, power spectrum of LFP signal.

K^+_{OUT}, Cl^-_{IN}, and neuronal firing resulted in a continued increase in neuronal firing and synchrony. We note that changes in internal chloride levels in PYs were relatively small, consisting in a 1 mM increase induced a depolarizing shift of 2–3 mV in the GABAergic reversal potential (Fig. 5*C*). Indeed the resulting decrease of inhibitory processes in the network induced pathologically synchronous bursting in both PY and IN populations.

We compared seizure dynamics in the model and experiment by analyzing normalized power spectra of the corresponding LFPs during the epileptic oscillations (Fig. 5*D*). A strong peak at 4 Hz in both cases corresponds to the principal frequency with several harmonic peaks. The LFP spectrum of the model captures the main frequency peak and $1/f$ behavior (Buzsáki et al., 2012). Oscillations at frequencies >40 Hz were not prominent. While our model did not capture all aspects of experimental traces (Fig. 5*B*, insets), many aspects of the LFP signal and power spectrum during the seizure were well matched (Fig. 5*D*). Thus accumulation of K^+_{OUT} and Cl^-_{IN} in the subicular PY–IN network with ≥30% KCC2(−) cells produces a pattern of activity similar to that recorded experimentally from human epileptic subiculum.

Analysis of epileptiform oscillations

The stability of epileptic network oscillations was assessed over a range of model parameters in simulations with 30% KCC2(−) PYs in the network. A seizure detection algorithm was applied to the model LFP to capture the moment of seizure initiation. Since the frequency of population bursts may change during the course of a seizure, we used the initial oscillation frequency at seizure onset, corresponding to the peak of the power spectrum (Fig. 5*D*). We found that this frequency decreases with the number of KCC2(−) cells (Fig. 6*A*). Bursting became slower as the duration of population bursts decreased, resulting in an increased interburst interval. This effect does not conform to a decrease in seizure activity since the prominence of population bursts increases with their duration.

With a stimulus equivalent to 8 mM extracellular potassium, the network tolerates ≤25% KCC2(−) cells before epileptic bursting emerges (Fig. 6*A*). At these lower levels, gamma frequency oscillations are generated (Fig. 4). Epileptic oscillations were produced as the proportion of KCC2(−) cells exceeded a critical threshold (Fig. 6*A*, dashed line). Higher proportions resulted in a faster transition to epileptic activity. For instance, with >40% of KCC2(−) cells, activity became pathological in <5 s (Fig. 6*A*).

The strength of synaptic conductances may be an especially important factor in the initiation of seizure-like activity. We examined the effect of varying these parameters in a network with a suprathreshold proportion of 30% KCC2(−) cells (cf. Marder

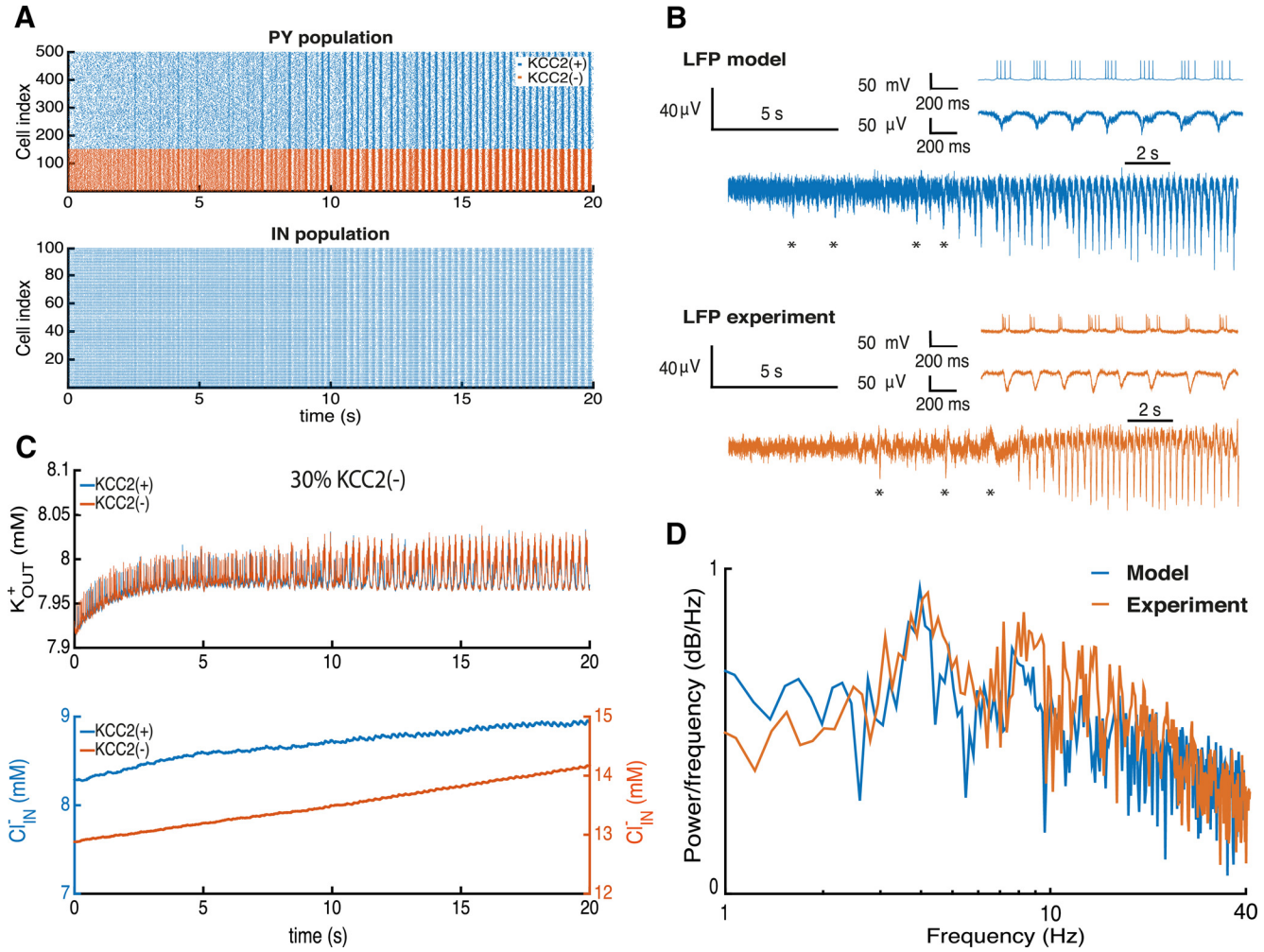

Figure 5. KCC2(−) pathology in the subiculum circuit. ***A***, Raster plot of firing in PYs and INs during seizure initiation. ***B***, LFP computed from the network and experimental LFP recordings. ***C***, Extracellular potassium, K^+_{OUT}, and intracellular chloride, Cl^-_{IN}, changes during seizure initiation. ***D***, Power spectrum of the LFP from the model and experimental recordings.

and Taylor, 2011). Mean values of synaptic parameters were altered and expressed as a percentage of the initial mean (Fig. 6, caption). We found large regions of parameter space corresponding to both resting state and epileptic oscillations (Fig. 6*B*). In the black region, the network generated oscillations at various frequencies, while in the white region epileptic oscillations were generated at 1–10 Hz for different synaptic parameter combinations. In general, the mean strength of AMPA-mediated recurrent PY–PY synapses governed the seizure-initiation threshold (Fig. 6*B*). In contrast, increasing the mean strength of excitatory synapses made with IN inhibitory cells tended to suppress ictal-like discharges. Similarly, increasing the strength of inhibitory synapses (GABA IN–PY) tended to reduce epileptic activity (Fig. 6*B*).

We also examined the effects of reducing the inhibitory synaptic parameters to zero for comparison with experiments using the $GABA_A$ receptor antagonist bicuculline (Fig. 6*C*, left). Suppressing GABAergic signaling in the model caused the network to generate periodic population bursts at ~1 Hz (Traub et al., 1987; de la Prida et al., 2006; Huberfeld et al., 2011). LFP oscillations became phase-locked with PY activity (Fig. 6*C*, right). The simulated network oscillation resulted from an interplay between recurrent excitation within the PY population and intrinsic neuronal currents I^K_{Ca} and I_{Ca} (Traub et al., 1987; Jung et al., 2001), which depend on intracellular Ca^{2+} dynamics. While the shape of the LFP differed to some extent, these data reflected the characteristic frequency of population events.

Thus, the presence of a threshold proportion of KCC2(−) cells has robust proictal effects evident over a range of excitatory and inhibitory synaptic strengths. Increasing synaptic inhibition reduces ictal-like activity and increasing recurrent excitation favors seizure-like events.

KCC2(−) pathology in the subiculum circuit with endogenous potassium

Using our model, we were able to separate the K^+_{OUT} and Cl^-_{IN} contributions to seizure initiation. In the intact brain, extracellular potassium levels depend on network activity, glial buffering, diffusion, and the Na-K pump (Bazhenov et al., 2004). To recreate this scenario in our computational model, we simulated this condition by eliminating the extracellular potassium in the bath with a compensatory increase in the input to PYs and IN cells at an intensity that generated sustained activity at physiological firing frequencies (Fig. 4). In these conditions, the presence of 40% of KCC2(−) PYs sufficed to generate epileptic oscillations (Fig. 7*A*). As in simulations using extracellular potassium as a stimulus (Fig. 5), high-frequency PY activity led to the gradual emergence of synchronicity in the network with population bursts as during ictal discharges.

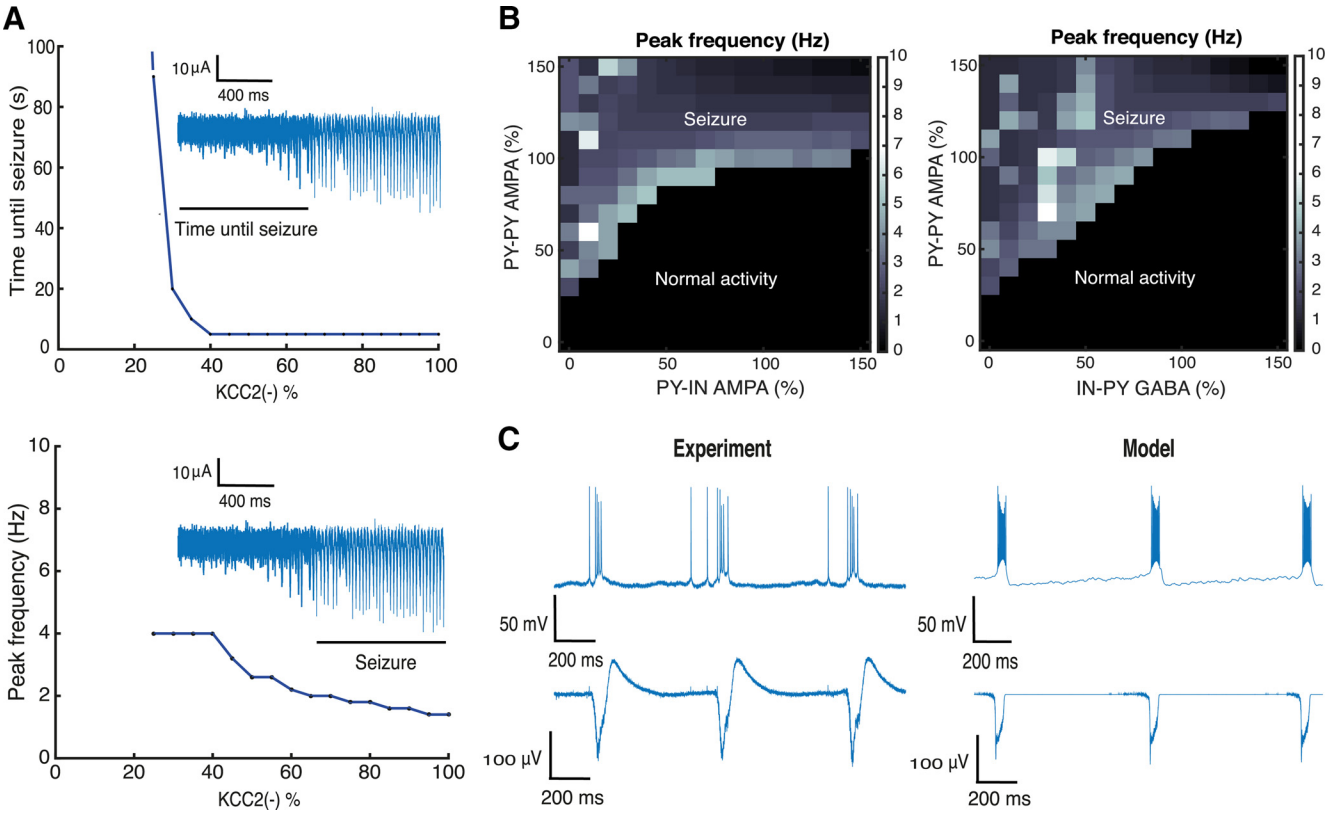

Figure 6. Analysis of epileptic oscillations. ***A***, Relations between the number of KCC2(−) cells in the network, and time until seizure initiation and peak frequency of LFP spectrum. The insets show characteristic LFP traces. ***B***, LFP peak frequency as a function of the mean strength of AMPA and GABA conductances in the network. ***C***, Population bursts generated after blocking inhibition in the model and experimental records (block with bicuculline). Synaptic conductances were varied from 0 to 150%: PY–PY, 0–2.25 nS/cm^2; PY–IN, 0–1.5 nS/cm^2; IN–PY, 0–1.05 nS/cm^2.

Ictal activity emerges after an increase in firing of both PYs and IN cells induces a progressive increase in K^+_{OUT} and Cl^-_{IN} levels (Fig. 7*C*). The resulting excitation–inhibition imbalance induced the emergence of synchronous bursting activity after 12 s. Extracellular potassium K^+_{OUT} levels then rose rapidly due to high-frequency firing of PYs. The positive feedback between firing and potassium levels continues to increase neuronal excitability and synchrony. Intracellular chloride levels Cl^-_{IN} also increased with IN cell firing, repetitive activation of inhibitory synapses, and a depolarizing shift in the GABA reversal potential in PYs.

Simulated LFP activity reflected firing of PYs (Fig. 7*B*) as with the elevated potassium stimulus (Fig. 5*B*). The power spectrum of LFP signals showed a maximum near 8 Hz, corresponding to the interburst interval (inset) with more peaks than in the elevated potassium simulations (Fig. 5*B*) but with a comparable general shape. Just as before, we found that a threshold proportion of ≥40% of KCC2(−) PYs was needed for seizure initiation (Fig. 7*D*). Oscillation frequency decreased as the proportion increased (Fig. 6*A*) and with >90% of KCC2(−) cells longer epileptic bursts were generated at frequencies of ~0.4 Hz.

Thus, accumulation of extracellular potassium and intracellular chloride induced seizure-like oscillations at endogenous potassium levels when the network contains a suprathreshold proportion of KCC2(−) PYs. Reducing the extracellular potassium preserved synchrony and oscillations were shifted to a higher frequency.

Dynamic elimination of the KCC2(−) pathology prevents seizure

As a final test, we asked whether restoring chloride homeostasis in an epileptic network at endogenous potassium concentrations could suppress epileptic synchrony. The network was initialized in conditions where epileptic oscillations were generated (Fig. 8) and after 5 s KCC2 function was restored in all KCC2(−) cells. The return to full KCC2 function slowly decreased synchrony in the PY and IN populations (Fig. 8*A*), transforming network activity after 45 s into stable, asynchronous firing corresponding to normal activity (Fig. 8*B*).

Restoring KCC2 function, restored potassium and chloride homeostasis. Internal chloride Cl^-_{IN} was reduced to 4.1 mM and external potassium K^+_{OUT} fell to 4 mM (Fig. 8*C*). A reduction in internal PY chloride levels reduced the excitatory drive to IN cells, and so reduced release from GABAergic synapses, further decreasing internal chloride in KCC2(+) as well as KCC2(−) PYs. Excitation–inhibition balance in the network was restored and neuronal synchrony reduced. Lower rates of PY firing led to reduced levels of extracellular potassium (Fig. 8*A*,*B*). We noted a biphasic decay in extracellular potassium and internal chloride levels (Fig. 8*C*, at ~40 s). It reflects the time point at which synchronous burst firing ceased. Ion concentrations were rapidly reestablished after this point. Restoring KCC2 function reverses epileptic oscillations in networks with ≤100% of KCC2(−) PYs and is equally effective in simulations with fixed K^+_{OUT} ≤8 mM (results not shown).

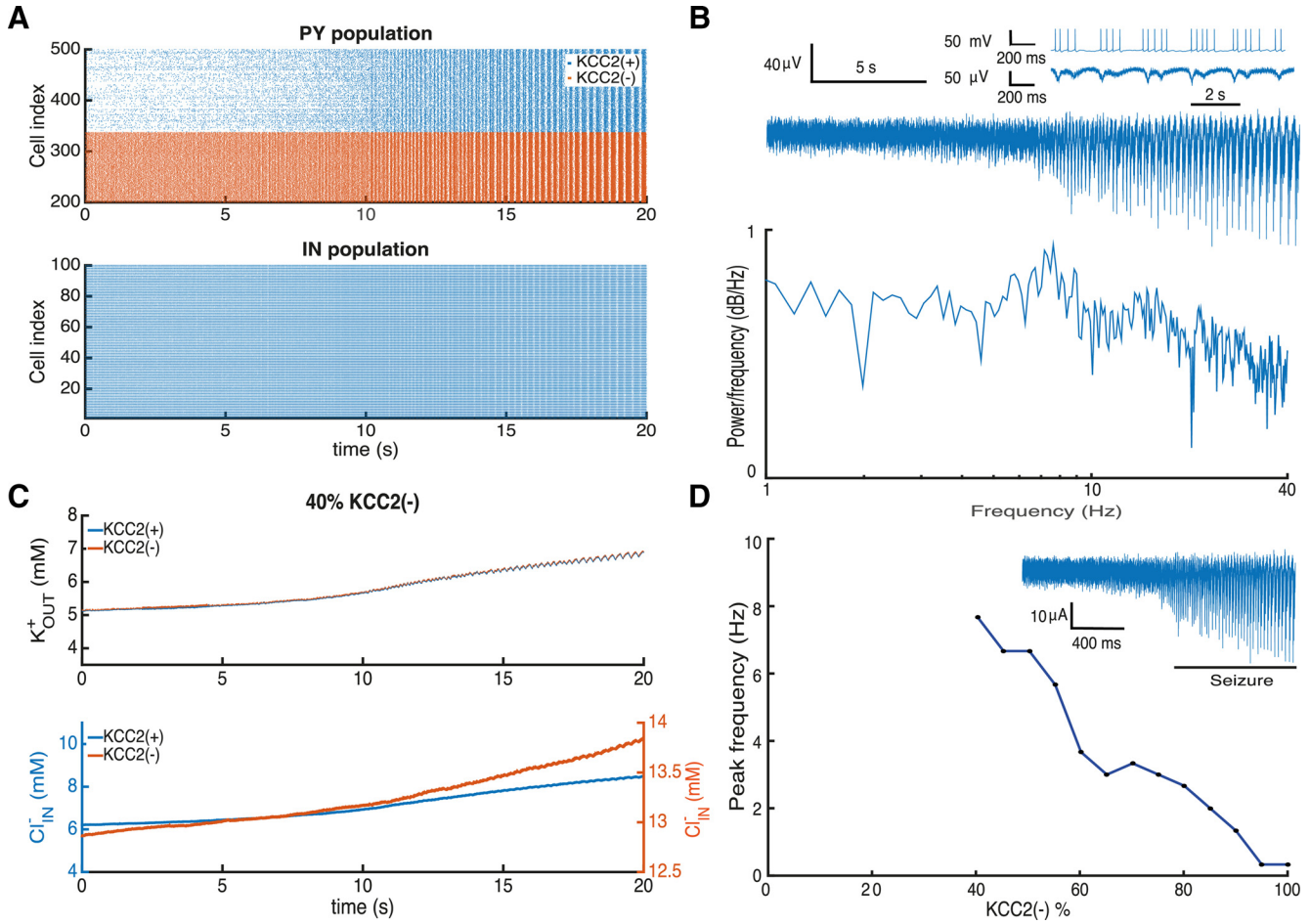

Figure 7. Adding KCC2(−) cells to the network with endogenous ion concentrations leads to the development of pathological oscillations ***A***, Activity of PYs and INs during seizure initiation. ***B***, LFP trace computed from neuronal activity and corresponding power spectrum. Inset, PY activity during the seizure. ***C***, Changes in the extracellular potassium, K^+_{OUT}, and intracellular chloride, Cl^-_{IN}, concentrations during seizure initiation. ***D***, Seizure frequency plotted against the proportion of KCC2(−) cells. The inset shows a typical LFP signal.

The recovery of network function after KCC2 restoration is evident in LFP power spectra (Fig. 8*D*). A characteristic peak in the LFP spectrum during seizure activity (Fig. 7*A*) is suppressed and the spectrum transformed to a $1/f$ type (Bédard and Destexhe, 2009) when asynchronous firing re-emerges.

Discussion

In this modeling study, we asked how the absence of KCC2 in some PYs might contribute to the generation of ictal-like activity in the human epileptic subiculum. The absence of KCC2 in simulated neurons results in a depolarizing shift of the reversal potential for responses to GABA. KCC2(−) neurons displayed an exaggerated persistent burst firing in response to elevated external potassium. In a network model with realistic subicular synaptic connectivity, epileptic oscillations developed when a critical proportion of KCC2(−) neurons were included. Simulated field potentials possessed a similar time course and frequency components to experimental data. Ictal-like activity was stable over a range of values for excitatory and inhibitory synaptic conductances, was generated with either fixed or endogenous levels of external potassium, and was blocked by restoring KCC2 activity. These data suggest that a defect in KCC2 expression or function in a minority of PYs could suffice to generate seizures.

Intracellular chloride homeostasis in PYs

The cotransporter KCC2 controls both chloride and potassium levels in neurons and is suggested to contribute to seizure initiation (Huberfeld et al., 2011; Zhang et al., 2011). There are several animal models incorporating the KCC2 deficiency (Hübner et al., 2001; Woo et al., 2002; Hekmat-Scafe et al., 2006), but their application for human studies is not straightforward. KCC2 is especially significant for synaptic responses to GABA, which may depolarize neurons during early development (Ben-Ari, 2002). At this stage, chloride homeostasis depends largely on the NKCC1 cotransporter, but later as KCC2 is expressed, responses to GABA become hyperpolarizing (Khalilov et al., 1999; Rivera et al., 1999; Payne et al., 2003). Multiple other factors, including pH, HCO_3, and CO_2, control responses to GABA (Dulla et al., 2005) and may be modified during epileptic activities, including febrile seizures (Schuchmann et al., 2009; Tolner et al., 2011). Local impermeant anions may also contribute to basal intracellular chloride (Glykys et al., 2014). Chloride levels also increase as inhibitory synapses are repetitively activated due to IN activity before and during ictal behaviors in the hippocampus (Isomura et al., 2003; Fujiwara-Tsukamoto et al., 2007; Lillis et al., 2012) and neocortex (Dietzel and Heinemann, 1986; Dietzel et al., 1989).

Our model did not include several factors contributing to chloride homeostasis that may be significant. The NKCC1 cotransporter has been shown to be involved in focal epilepsies (Huberfeld et al., 2007, 2011; Pallud et al., 2014). It appears to be upregulated and its blockade controls both interictal and ictal epileptic activities. The upregulation of NKCC1 results in the

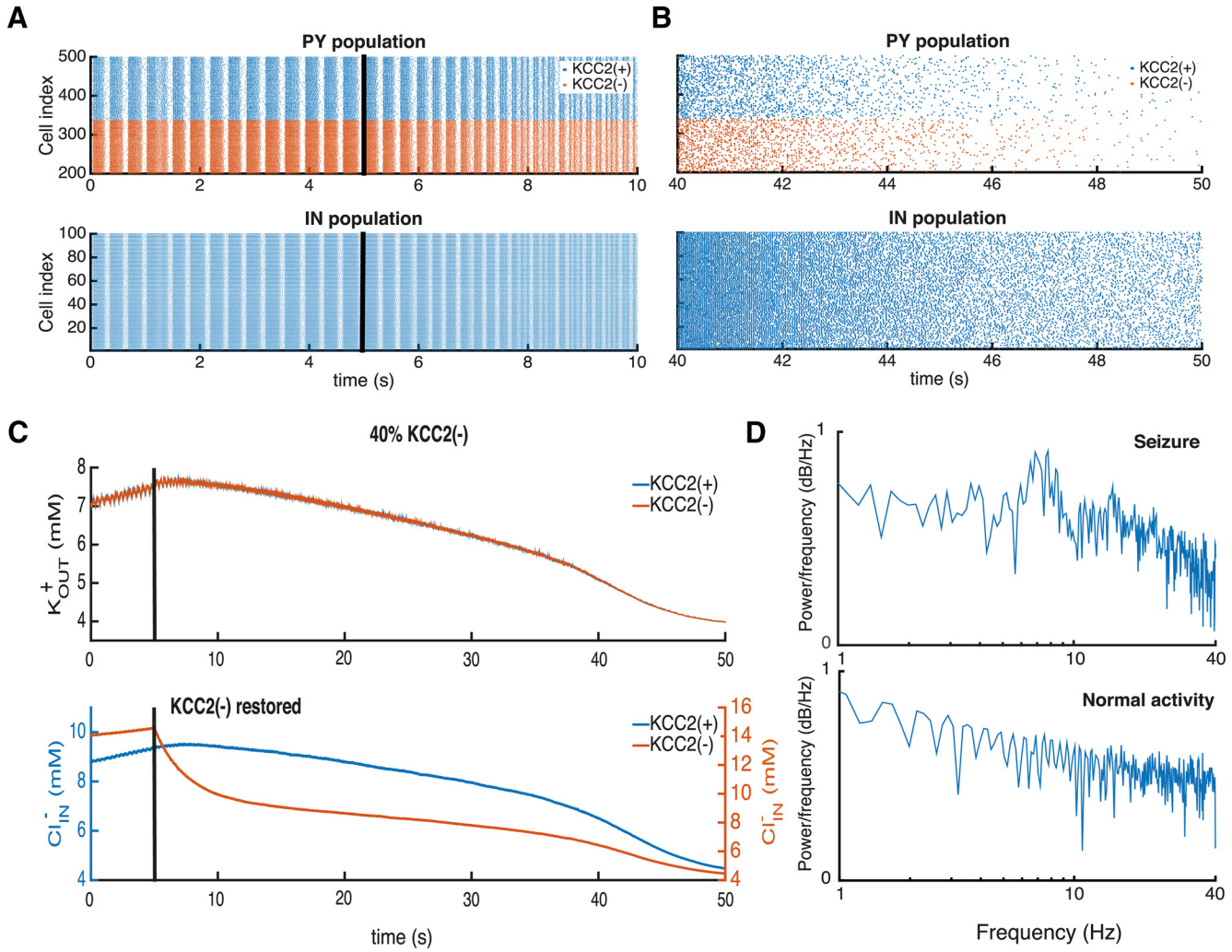

Figure 8. Restoring KCC2(−) function with realistic ionic levels prevents seizure. ***A***, ***B***, raster plots of PY and IN activities during seizure oscillations are shown on the left. Those during the transition to normal activity after restoring KCC2 function (black line at 5 s) are shown on the right. ***C***, Changes in the extracellular potassium, K^+_{OUT}, and intracellular chloride, Cl^-_{IN}, concentrations after restoring KCC2 function, at the black line. ***D***, LFP power spectra during epileptic oscillations and after KKC2 function was restored in KCC2(−) cells.

increase of GABA reversal potential level so as the downregulation of KCC2 (results not shown). The absence of NKCC1 in the present model highlights the crucial effect of reduced KCC2 function or expression on ictogenesis. The anion exchangers and NKCC1 undoubtedly contribute to the intracellular chloride homeostasis (Doyon et al., 2016). But that issue is beyond the scope of our study, which concentrates on the crucial role of KCC2 with respect to K and Cl. Concentration changes of bicarbonate ions via anion exchangers, such as AE3 (Hentschke et al., 2006) and EAAT3-4 (Deisz et al., 2014), could significantly affect the chloride extrusion rate. However, the reversal potential of GABAergic currents in neurons of diseased human neocortex tends to be depolarized from rest (Deisz et al., 2011, 2014; Pallud et al., 2014). KCC2 activity is consistently reduced but some degree of Cl^- extrusion may persist due to AE3 or EAAT3-4 (Deisz et al., 2011, 2014). However, currently there are few data on the function of residual anion exchangers in the subiculum. Future studies should evaluate the contribution of these mechanisms together with intracellular chloride.

The present KCC2 model used in this study (Doyon et al., 2011) is based on the assumption that chloride clearance is proportional to the free energy available for ion transport that could be estimated as potential difference between V_K and V_{Cl} (Staley and Proctor, 1999). More complex KCC2 models (Chang and Fujita, 1999) describe chloride clearance in more detail, yet they would provide substantially similar results if they are based on the same data (Staley and Proctor, 1999; Lewin et al., 2012).

Extracellular potassium contribution to epileptiform activity

Elevated extracellular potassium levels were initially associated with seizure initiation (Fertziger and Ranck, 1970; Ranck, 1970; Dietzel and Heinemann, 1986; Dietzel et al., 1989). External potassium increases not only at the seizure-onset site but also along pathways of seizure spread. However, it may be difficult to measure timing of potassium kinetics precisely due to slow response of ion-sensitive electrodes. Seizure threshold potassium levels have been defined in the hippocampus but are less clear in the neocortex (Antonio et al., 2016). Despite finding in more recent studies (Bazhenov et al., 2004; D'Antuono et al., 2004; Fröhlich et al., 2008b; Ullah et al., 2009; Wei et al., 2014), it still remains unclear whether an accumulation of extracellular potassium is a cause or a consequence of ictal behavior.

Our simulations suggest that an increase in extracellular potassium alone did not lead to seizure activity, at least at 8 mM. Even so, the KCC2 transporter clearly increases external potassium and contributes to the enhanced, self-sustained firing of

PYs. In this context, it is interesting that the KCC2 pathology in epileptic human tissue affects only a minority of PYs (Huberfeld et al., 2007). In certain conditions potassium extrusion from KCC2(+) neurons may be equally important in the generation of ictal events (Hamidi and Avoli, 2015). Our results therefore suggest that the increase of extracellular potassium (Antonio et al., 2016) and intracellular chloride in the subiculum contribute to seizure initiation. These predictions should be tested by simultaneously measuring these parameters in slice experiments during seizure initiation.

Extracellular levels of potassium also affect GABAergic signaling. Since the KCC2 cotransporter operates close to a thermodynamic equilibrium (Payne, 1997), external potassium levels are closely linked to basal levels of intracellular chloride, thus defining the efficacy of GABAergic signaling (Khalilov et al., 1999). Even small increases in external potassium induce significant neuronal chloride accumulation (Payne et al., 2003), thus reducing the efficacy of GABAergic synapses.

The role of the KCC2(−) cells

Our data show that including a minority of KCC2(−) cells in a simulated subicular network induced ictal-like epileptic oscillations (Figs. 5, 7). Restoring function in these neurons blocked the activity (Fig. 8). The presence of KCC2(−) cells stimulated IN firing, thus provoking a feedback increase in intracellular chloride in KCC2(−) PYs. The resulting imbalance in excitation and inhibition led to generation of epileptic oscillations by the network. These data mirror the experimental finding of strong IN firing at seizure initiation (Gnatkovsky et al., 2008). Thus an activity-dependent chloride accumulation in PYs due to intensive IN firing (Lillis et al., 2012) contributes to a gradual failure of an inhibitory restraint as seizures propagate (Trevelyan et al., 2007; Schevon et al., 2012).

Elevated internal chloride levels in KCC2(−) PYs resulted in a depolarized resting potential and GABAergic reversal potential compared with KCC2(+) cells. The resulting persistent increase in the excitability of KCC2(−) cells may induce plasticity in the strength or number of recurrent excitatory connections made by these neurons. Further work should address possible differences in synaptic function and connectivity between KCC2(−) and KCC2(+) PYs.

Our data showed that restoring KCC2 function in PYs effectively blocked seizure activity in the network (Fig. 8). Thus pharmaceutical strategies to restore or strengthen chloride homeostasis (Gagnon et al., 2013) may be a useful therapeutic tool in certain epileptic syndromes.

It has been recently found that addition of the specific KCC2 blocker VU0463271 to mouse hippocampal slices provokes generation of epileptic activity (Sivakumaran et al., 2015). This study is consistent with our model and conclusions based on human hippocampal sclerotic tissue (Huberfeld et al., 2007). In contrast to this, other authors (Hamidi and Avoli, 2015) showed that the blockade of KCC2 with another compound, VU0240551, prevents generation of ictal discharges in similar experimental conditions. Nonetheless we found that downregulation of the KCC2 in the network provides a larger increase of excitability due to Cl^-_{IN} accumulation leading to ictal discharge generation (Figs. 5, 7). Therefore we predict that the epileptogenic effect of KCC2 is mostly due to failure of chloride regulation, while the increase of excitability due to extracellular potassium released by KCC2 (Viitanen et al., 2010) has a smaller effect on seizure initiation. We believe that further development of more specific KCC2 blockers would help resolve this controversial issue.

Conclusions

Epilepsy is a complex disease involving dynamic interactions between many different elements of an epileptic brain (Lytton, 2008; Jirsa et al., 2014; Proix et al., 2014; Naze et al., 2015). In this work we have characterized one pathological pathway associated with chloride and potassium homeostasis in the human subiculum. Recent work on the epileptic peritumoral cortex (Pallud et al., 2014), cortical dysplasias, and tuberous sclerosis (Talos et al., 2012) suggests that changes in chloride-potassium cotransport contribute to epileptic syndromes beyond the sclerotic hippocampal formation. Further modeling and experimental work may lead to a deeper understanding of the mechanisms involved and help define new therapeutic targets.

References

Alger BE, Nicoll RA (1982) Feed-forward dendritic inhibition in rat hippocampal pyramidal cells studied in vitro. J Physiol 328:105–123. CrossRef Medline

Antonio LL, Anderson ML, Angamo EA, Gabriel S, Klaft ZJ, Liotta A, Salar S, Sandow N, Heinemann U (2016) In vitro seizure like events and changes in ionic concentration. J Neurosci Methods 260:33–44. CrossRef Medline

Barreto E, Cressman JR (2011) Ion concentration dynamics as a mechanism for neuronal bursting. J Biol Phys 37:361–373. CrossRef Medline

Bazhenov M, Timofeev I, Steriade M, Sejnowski TJ (2004) Potassium model for slow (2–3 Hz) in vivo neocortical paroxysmal oscillations. J Neurophysiol 92:1116–1132. CrossRef Medline

Bédard C, Destexhe A (2009) Macroscopic models of local field potentials and the apparent 1/f noise in brain activity. Biophys J 96:2589–2603. CrossRef Medline

Beghi E, Berg A, Carpio A, Forsgren L, Hesdorffer DC, Hauser WA, Malmgren K, Shinnar S, Temkin N, Thurman D, Tomson T. (2005) Comment on epileptic seizures and epilepsy: definitions proposed by the International League Against Epilepsy (ILAE) and the International Bureau for Epilepsy (IBE). Epilepsia 46:1698–1699; author reply 1701–1702. CrossRef Medline

Ben-Ari Y (2002) Excitatory actions of gaba during development: the nature of the nurture. Nat Rev Neurosci:728–739. Medline

Böhm C, Peng Y, Maier N, Winterer J, Poulet JF, Geiger JR, Schmitz D (2015) Functional diversity of subicular principal cells during hippocampal ripples. J Neurosci 35:13608–13618. CrossRef Medline

Brunel N, Wang XJ (2001) Effects of neuromodulation in a cortical network model of object working memory. J Comput Neurosci 11:63–85. CrossRef Medline

Buzsáki G, Anastassiou CA, Koch C (2012) The origin of extracellular fields and currents—EEG, ECoG, LFP and spikes. Nat Rev Neurosci 13:407–420. CrossRef Medline

Chang H, Fujita T (1999) A numerical model of the renal distal tubule. Am J Physiol 276:F931–F951. Medline

Chizhov AV (2002) Model of evoked activity of populations of neurons in the hippocampus (in Russian). Biofizika 47:1086–1094. Medline

Chizhov AV, Sanchez-Aguilera A, Rodrigues S, de la Prida LM (2015) Simplest relationship between local field potential and intracellular signals in layered neural tissue. Phys Rev E Stat Nonlin Soft Matter Phys 92:062704. CrossRef Medline

Cohen I, Navarro V, Clemenceau S, Baulac M, Miles R (2002) On the origin of interictal activity in human temporal lobe epilepsy in vitro. Science 298:1418–1421. CrossRef Medline

Colling SB, Stanford IM, Traub RD, Jefferys JGR, Jackson J, Goutagny R, Williams S, Stanford IANM (1998) Limbic gamma rhythms I. Phase-locked oscillations in hippocampal CA1 and subiculum limbic gamma rhythms. J Neuroph 80:155–161. Medline

Cressman JR Jr, Ullah G, Ziburkus J, Schiff SJ, Barreto E (2009) The influence of sodium and potassium dynamics on excitability, seizures, and the stability of persistent states: I. Single neuron dynamics. J Comput Neurosci 26:159–170. CrossRef Medline

D'Antuono M, Louvel J, Köhling R, Mattia D, Bernasconi A, Olivier A, Turak B, Devaux A, Pumain R, Avoli M (2004) GABA A receptor-dependent synchronization leads to ictogenesis in the human dysplastic cortex. Brain 127:1626–1640. CrossRef Medline

de la Prida LM, Huberfeld G, Cohen I, Miles R (2006) Threshold behavior in

the initiation of hippocampal population bursts. Neuron 49:131–142. CrossRef Medline

Deisz RA, Lehmann TN, Horn P, Dehnicke C, Nitsch R (2011) Components of neuronal chloride transport in rat and human neocortex. J Physiol 589:1317–1347. CrossRef Medline

Deisz RA, Wierschke S, Schneider UC, Dehnicke C (2014) Effects of VU0240551 a novel KCC2 antagonist, and DIDS on chloride homeostasis of neocortical neurons from rats and humans. Neuroscience 277:831–841. CrossRef Medline

Demont-Guignard S, Benquet P, Gerber U, Biraben A, Martin B, Wendling F (2012) Distinct hyperexcitability mechanisms underlie fast ripples and epileptic spikes. Ann Neurol 71:342–352. CrossRef Medline

Dietzel I, Heinemann U (1986) Dynamic variations of the brain cell microenvironment in relation to neuronal hyperactivity. Ann NY Acad Sci 481:72–86. CrossRef Medline

Dietzel I, Heinemann U, Lux HD (1989) Relations between slow extracellular potential changes, glial potassium buffering, and electrolyte and cellular volume changes during neuronal hyperactivity in cat brain. Glia 2:25–44. CrossRef Medline

Doyon N, Prescott SA, Castonguay A, Godin AG, Kröger H, De Koninck Y (2011) Efficacy of synaptic inhibition depends on multiple, dynamically interacting mechanisms implicated in chloride homeostasis. PLoS Comput Biol 7:e1002149. CrossRef Medline

Doyon N, Vinay L, Prescott SA, De Koninck Y (2016) Chloride regulation: a dynamic equilibrium crucial for synaptic inhibition. Neuron 89:1157–1172. CrossRef Medline

Dulla CG, Dobelis P, Pearson T, Frenguelli BG, Staley KJ, Masino SA (2005) Adenosine and ATP link PCO2 to cortical excitability via pH. Neuron 48:1011–1023. CrossRef Medline

Fertziger AP, Ranck JB Jr (1970) Potassium accumulation in interstitial space during epileptiform seizures. Exp Neurol 26:571–585. CrossRef Medline

Fisher RS, Pedley TA, Prince DA (1976) Kinetics of potassium movement in normal cortex. Brain Res 101:223–237. Medline

Fisher RS, van Emde Boas W, Blume W, Elger C, Genton P, Lee P, Engel J Jr (2005) Epileptic seizures and epilepsy: definitions proposed by the International League Against Epilepsy (ILAE) and the International Bureau for Epilepsy (IBE). Epilepsia 46:470–472. CrossRef Medline

Florence G, Dahlem MA, Almeida AC, Bassani JW, Kurths J (2009) The role of extracellular potassium dynamics in the different stages of ictal bursting and spreading depression: a computational study. J Theor Biol 258:219–228. CrossRef Medline

Fröhlich F, Bazhenov M, Sejnowski TJ (2008a) Pathological effect of homeostatic synaptic scaling on network dynamics in diseases of the cortex. J Neurosci 28:1709–1720. CrossRef Medline

Fröhlich F, Bazhenov M, Iragui-Madoz V, Sejnowski TJ (2008b) Potassium dynamics in the epileptic cortex: new insights on an old topic. Neuroscientist 14:422–433. CrossRef Medline

Fujiwara-Tsukamoto Y, Isomura Y, Imanishi M, Fukai T, Takada M (2007) Distinct types of ionic modulation of GABA actions in pyramidal cells and interneurons during electrical induction of hippocampal seizure-like network activity. Eur J Neurosci 25:2713–2725. CrossRef Medline

Fujiwara-Tsukamoto Y, Isomura Y, Imanishi M, Ninomiya T, Tsukada M, Yanagawa Y, Fukai T, Takada M (2010) Prototypic seizure activity driven by mature hippocampal fast-spiking interneurons. J Neurosci 30:13679–13689. CrossRef Medline

Gagnon M, Bergeron MJ, Lavertu G, Castonguay A, Tripathy S, Bonin RP, Perez-Sanchez J, Boudreau D, Wang B, Dumas L, Valade I, Bachand K, Jacob-Wagner M, Tardif C, Kianicka I, Isenring P, Attardo G, Coull JA, De Koninck Y (2013) Chloride extrusion enhancers as novel therapeutics for neurological diseases. Nat Med 19:1524–1528. CrossRef Medline

Glykys J, Dzhala V, Egawa K, Balena T, Saponjian Y, Kuchibhotla KV, Bacskai BJ, Kahle KT, Zeuthen T, Staley KJ (2014) Local impermeant anions establish the neuronal chloride concentration. Science 343:670–675. CrossRef Medline

Gnatkovsky V, Librizzi L, Trombin F, de Curtis M (2008) Fast activity at seizure onset is mediated by inhibitory circuits in the entorhinal cortex in vitro. Ann Neurol 64:674–686. CrossRef Medline

Grafstein B (1956) Mechanism of spreading cortical depression. J Neurophysiol 19:154–171. Medline

Grisar T (1984) Glial and neuronal Na+-K+ pump in epilepsy. Ann Neurol 16[Suppl]):S128–S134. CrossRef Medline

Hamidi S, Avoli M (2015) KCC2 function modulates in vitro ictogenesis. Neurobiol Dis 79:51–58. CrossRef Medline

Hekmat-Scafe DS, Lundy MY, Ranga R, Tanouye MA (2006) Mutations in the K^+/Cl^- cotransporter gene *kazachoc* (*kcc*) increase seizure susceptibility in *Drosophila*. J Neurosci 26:8943–8954. CrossRef Medline

Hentschke M, Wiemann M, Hentschke S, Kurth I, Hermans-Borgmeyer I, Seidenbecher T, Jentsch TJ, Gal A, Hübner CA (2006 Jan 1) Mice with a targeted disruption of the Cl−/HCO3− exchanger AE3 display a reduced seizure threshold. Mol Cell Biol 26:182–191. CrossRef Medline

Hübel N, Dahlem MA (2014) Dynamics from seconds to hours in Hodgkin–Huxley model with time-dependent ion concentrations and buffer reservoirs. PLoS Comput Biol 10:e1003941. CrossRef Medline

Huberfeld G, Wittner L, Clemenceau S, Baulac M, Kaila K, Miles R, Rivera C (2007) Perturbed chloride homeostasis and GABAergic signaling in human temporal lobe epilepsy. J Neurosci 27:9866–9873. CrossRef Medline

Huberfeld G, Menendez de la Prida L, Pallud J, Cohen I, Le Van Quyen M, Adam C, Clemenceau S, Baulac M, Miles R (2011) Glutamatergic pre-ictal discharges emerge at the transition to seizure in human epilepsy. Nat Neurosci 14:627–634. CrossRef Medline

Hübner CA, Stein V, Hermans-Borgmeyer I, Meyer T, Ballanyi K, Jentsch TJ (2001) Disruption of KCC2 reveals an essential role of K-Cl cotransport already in early synaptic inhibition. Neuron 30:515–524. CrossRef Medline

Huchzermeyer C, Albus K, Gabriel HJ, Otáhal J, Taubenberger N, Heinemann U, Kovács R, Kann O (2008) Gamma oscillations and spontaneous network activity in the hippocampus are highly sensitive to decreases in pO2 and concomitant changes in mitochondrial redox state. J Neurosci 28:1153–1162. CrossRef Medline

Isomura Y, Sugimoto M, Fujiwara-Tsukamoto Y, Yamamoto-Muraki S, Yamada J, Fukuda A (2003) Synaptically activated Cl− accumulation responsible for depolarizing GABAergic responses in mature hippocampal neurons. J Neurophysiol 90:2752–2756. CrossRef Medline

Jackson J, Goutagny R, Williams S (2011) Fast and slow γ rhythms are intrinsically and independently generated in the subiculum. J Neurosci 31:12104–12117. CrossRef Medline

Jedlicka P, Deller T, Gutkin BS, Backus KH (2011) Activity-dependent intracellular chloride accumulation and diffusion controls GABA(A) receptor-mediated synaptic transmission. Hippocampus 21:885–898. CrossRef Medline

Jensen MS, Azouz R, Yaari Y (1994) Variant firing patterns in rat hippocampal pyramidal cells modulated by extracellular potassium. J Neurophysiol 71:831–839. Medline

Jirsa VK, Stacey WC, Quilichini PP, Ivanov AI, Bernard C (2014) On the nature of seizure dynamics. Brain 137:2210–2230. CrossRef Medline

Jung HY, Staff NP, Spruston N (2001) Action potential bursting in subicular pyramidal neurons is driven by a calcium tail current. J Neurosci 21:3312–3321. Medline

Kager H, Wadman WJ, Somjen GG (2000) Simulated seizures and spreading depression in a neuron model incorporating interstitial space and ion concentrations. J Neurophysiol 84:495–512. Medline

Kager H, Wadman WJ, Somjen GG (2007) Seizure-like afterdischarges simulated in a model neuron. J Comput Neurosci 22:105–128. CrossRef Medline

Kaila K, Voipio J (1987) Postsynaptic fall in intracellular pH induced by GABA-activated bicarbonate conductance. Nature 330:163–165. CrossRef Medline

Khalilov I, Dzhala V, Ben-Ari Y, Khazipov R (1999) Dual Role of GABA in the neonatal rat hippocampus. Dev Neurosci 21:310–319. Medline

Kraig RP, Nicholson C (1978) Extracellular ionic variations during spreading depression. Neuroscience 3:1045–1059. CrossRef Medline

Krishnan GP, Bazhenov M (2011) Ionic dynamics mediate spontaneous termination of seizures and postictal depression state. J Neurosci 31:8870–8882. CrossRef Medline

LeBeau FE, Towers SK, Traub RD, Whittington MA, Buhl EH (2002) Fast network oscillations induced by potassium transients in the rat hippocampus in vitro. J Physiol 542:167–179. CrossRef Medline

Lewin N, Aksay E, Clancy CE (2012) Computational modeling reveals dendritic origins of GABAA-mediated excitation in CA1 pyramidal neurons. PLoS One 7:e47250. CrossRef Medline

Lillis KP, Kramer MA, Mertz J, Staley KJ, White JA (2012) Pyramidal cells accumulate chloride at seizure onset. Neurobiol Dis 47:358–366. CrossRef Medline

Lytton WW (2008) Computer modeling of epilepsy. Nat Rev Neurosci 9:626–637. Medline

Mainen ZF, Sejnowski TJ (1996) Influence of dendritic structure on firing pattern in model neocortical neurons. Nature 382:363–366. CrossRef Medline

Marder E, Taylor AL (2011) Multiple models to capture the variability in biological neurons and networks. Nat Neurosci 14:133–138. CrossRef Medline

Naze S, Bernard C, Jirsa V (2015) Computational modeling of seizure dynamics using coupled neuronal networks: factors shaping epileptiform activity. PLoS Comput Biol 11:e1004209. CrossRef Medline

Pallud J, Le Van Quyen M, Bielle F, Pellegrino C, Varlet P, Labussiere M, Cresto N, Dieme MJ, Baulac M, Duyckaerts C, Kourdougli N, Chazal G, Devaux B, Rivera C, Miles R, Capelle L, Huberfeld G (2014) Cortical GABAergic excitation contributes to epileptic activities around human glioma. Sci Transl Med 6:244ra89. CrossRef Medline

Payne JA (1997) Functional characterization of the neuronal-specific K-Cl cotransporter: implications for [K+]o regulation. Am J Physiol 273: C1516–C1525. Medline

Payne JA, Rivera C, Voipio J, Kaila K (2003) Cation-chloride co-transporters in neuronal communication, development and trauma. Trends Neurosci 26:199–206. CrossRef Medline

Proix T, Bartolomei F, Chauvel P, Bernard C, Jirsa VK (2014) Permittivity coupling across brain regions determines seizure recruitment in partial epilepsy. J Neurosci 34:15009–15021. CrossRef Medline

Renart A, Moreno-Bote R, Wang XJ, Parga N (2007) Mean-driven and fluctuation-driven persistent activity in recurrent networks. Neural Comput 19:1–46. CrossRef Medline

Rivera C, Voipio J, Payne JA, Ruusuvuori E, Lahtinen H, Lamsa K, Pirvola U, Saarma M, Kaila K (1999) The K+/Cl− co-transporter KCC2 renders GABA hyperpolarizing during neuronal maturation. Nature 397:251–255. CrossRef Medline

Schevon CA, Weiss SA, McKhann G Jr, Goodman RR, Yuste R, Emerson RG, Trevelyan AJ (2012) Evidence of an inhibitory restraint of seizure activity in humans. Nat Commun 3:1060. CrossRef Medline

Schuchmann S, Vanhatalo S, Kaila K (2009) Neurobiological and physiological mechanisms of fever-related epileptiform syndromes. Brain Dev 31:378–382. CrossRef Medline

Sivakumaran S, Cardarelli RA, Maguire J, Kelley MR, Silayeva L, Morrow DH, Mukherjee J, Moore YE, Mather RJ, Duggan ME, Brandon NJ, Dunlop J, Zicha S, Moss SJ, Deeb TZ (2015) Selective inhibition of KCC2 leads to hyperexcitability and epileptiform discharges in hippocampal slices and *in vivo*. J Neurosci 35:8291–8296. CrossRef Medline

Staff NP, Jung HY, Thiagarajan T, Yao M, Spruston N (2000) Resting and active properties of pyramidal neurons in subiculum and CA1 of rat hippocampus. J Neurophysiol 84:2398–2408. Medline

Staley KJ, Proctor WR (1999) Modulation of mammalian dendritic GABA A receptor function by the kinetics of Cl− and HCO3− transport. J Physiol 519:693–712. CrossRef Medline

Staley KJ, Soldo BL, Proctor WR (1995) Ionic mechanisms of neuronal excitation by inhibitory GABAA receptors. Science 269:977–981. CrossRef Medline

Stanford IM, Traub RD, Jefferys JG (1998) Limbic gamma rhythms. II. Synaptic and intrinsic mechanisms underlying spike doublets in oscillating subicular neurons. J Neurophysiol 80:162–171. Medline

Talos DM, Sun H, Kosaras B, Joseph A, Folkerth RD, Poduri A, Madsen JR, Black PM, Jensen FE (2012) Altered inhibition in tuberous sclerosis and type IIb cortical dysplasia. Ann Neurol 71:539–551. CrossRef Medline

Tolner EA, Hochman DW, Hassinen P, Otáhal J, Gaily E, Haglund MM, Kubová H, Schuchmann S, Vanhatalo S, Kaila K (2011) Five percent CO_2 is a potent, fast-acting inhalation anticonvulsant. Epilepsia 52:104–114. CrossRef Medline

Traub RD, Miles R, Wong RK, Schulman LS, Schneiderman JH (1987) Models of synchronized hippocampal bursts in the presence of inhibition. II. Ongoing spontaneous population events. J Neurophysiol 58:752–764. Medline

Trevelyan AJ, Sussillo D, Yuste R (2007) Feedforward inhibition contributes to the control of epileptiform propagation speed. J Neurosci 27:3383–3387. CrossRef Medline

Ullah G, Schiff SJ (2009) Models of epilepsy. Scholarpedia 4:1409. CrossRef

Ullah G, Cressman JR Jr, Barreto E, Schiff SJ (2009) The influence of sodium and potassium dynamics on excitability, seizures, and the stability of persistent states. II. Network and glial dynamics. J Comput Neurosci 26:171–183. CrossRef Medline

Viitanen T, Ruusuvuori E, Kaila K, Voipio J (2010) The K+-Cl cotransporter KCC2 promotes GABAergic excitation in the mature rat hippocampus. J Physiol 588:1527–1540. CrossRef Medline

Volman V, Ben-Jacob E, Levine H (2007) The astrocyte as a gatekeeper of synaptic information transfer. Neural Comput 19:303–326. CrossRef Medline

Wallraff A, Köhling R, Heinemann U, Theis M, Willecke K, Steinhäuser C (2006) The impact of astrocytic gap junctional coupling on potassium buffering in the hippocampus. J Neurosci 26:5438–5447. CrossRef Medline

Wei Y, Ullah G, Schiff SJ (2014) Unification of neuronal spikes, seizures, and spreading depression. J Neurosci 34:11733–11743. CrossRef Medline

Wendling F, Bartolomei F, Mina F, Huneau C, Benquet P (2012) Interictal spikes, fast ripples and seizures in partial epilepsies—combining multilevel computational models with experimental data. Eur J Neurosci 36: 2164–2177. CrossRef Medline

Whittington MA, Traub RD, Kopell N, Ermentrout B, Buhl EH (2000) Inhibition-based rhythms: experimental and mathematical observations on network dynamics. Int J Psychophysiol 38:315–336. CrossRef Medline

Woo NS, Lu J, England R, McClellan R, Dufour S, Mount DB, Deutch AY, Lovinger DM, Delpire E (2002) Hyperexcitability and epilepsy associated with disruption of the mouse neuronal-specific K-Cl cotransporter gene. Hippocampus 12:258–268. CrossRef Medline

Zhang ZJ, Valiante TA, Carlen PL (2011) Transition to seizure: from "macro"- to "micro"-mysteries. Epilepsy Res 97:290–299. CrossRef Medline